© 2019. Published by The Company of Biologists Ltd | Development (2019) 146, dev175547. doi:10.1242/dev.175547

RESEARCH ARTICLE

PHF7 is a novel histone H2A E3 ligase prior to histone-to-protamine exchange during spermiogenesis

Xiukun Wang[1,*], Jun-Yan Kang[2,*], Leixin Wei[1,3,*], Xiaogan Yang[4,*], Hongduo Sun[5], Suming Yang[1], Lei Lu[1], Meng Yan[1], Meizhu Bai[1], Yanyan Chen[6], Juanjuan Long[6], Na Li[1], Dangsheng Li[7], Jing Huang[6], Ming Lei[6], Zhen Shao[5], Wen Yuan[3,‡], Erwei Zuo[4,8,‡], Kehuan Lu[4,‡], Mo-Fang Liu[2,‡] and Jinsong Li[1,‡]

ABSTRACT

Epigenetic regulation, including histone-to-protamine exchanges, controls spermiogenesis. However, the underlying mechanisms of this regulation are largely unknown. Here, we report that PHF7, a testis-specific PHD and RING finger domain-containing protein, is essential for histone-to-protamine exchange in mice. PHF7 is specifically expressed during spermiogenesis. PHF7 deletion results in male infertility due to aberrant histone retention and impaired protamine replacement in elongated spermatids. Mechanistically, PHF7 can simultaneously bind histone H2A and H3; its PHD domain, a histone code reader, can specifically bind H3K4me3/me2, and its RING domain, a histone writer, can ubiquitylate H2A. Thus, our study reveals that PHF7 is a novel E3 ligase that can specifically ubiquitylate H2A through binding H3K4me3/me2 prior to histone-to-protamine exchange.

KEY WORDS: Spermiogenesis, Histone-to-protamine exchange, PHF7, Histone H2A ubiquitylation, E3 ligase

INTRODUCTION

Spermatogenesis is a complex process that can be roughly divided into the mitotic phase, meiotic phase and post-meiotic phase (i.e. spermiogenesis) (Rathke et al., 2014). During spermiogenesis, haploid round spermatids undergo extensive morphological changes to become flagella-containing motile sperm through a 16-step process, including round spermatids (steps 1 to 8), elongating spermatids (steps 9 to 11), elongated or condensed spermatids (steps 12-14), and spermatozoa (steps 15-16) (Carrell and Aston, 2013; Meistrich and Hess, 2013). This dramatic differentiation process is precisely regulated by a number of epigenetic factors. In spermiogenesis, DNA-binding histones are first replaced by transition proteins (Tnp1 and Tnp2) and transition proteins are then replaced by protamines (Prm1 and Prm2) constituting the nuclear proteins of spermatozoa and mature sperm (Bao and Bedford, 2016; Rathke et al., 2014). Histone-to-protamine exchange is crucial for chromatin compaction and packaging of genome DNA into sperm head, an essential step for the formation of functional sperm. Previous studies have established a link between defective histone-to-protamine exchange and male infertility (Casas and Vavouri, 2014; Meistrich et al., 2003; Oliva, 2006); however, the molecular mechanisms underlying chromatin compaction are still poorly understood.

Ubiquitylation of histones, especially H2A and H2B, in developing male germ cells (Baarends et al., 1999; Jason et al., 2002) has been considered to be one of the important epigenetic marks involved in chromatin remodeling during spermatogenesis (Bao and Bedford, 2016; Govin et al., 2004; Rathke et al., 2014; Sheng et al., 2014). A previous study indicated that the E3 ligase RNF8 mediates H2B and/or H2A ubiquitylation in elongating spermatids, which induces H4K16 acetylation (downstream of H2B ubiquitination) and nucleosome removal (Lu et al., 2010). Intriguingly, we recently found that ubiquitylation-deficient mutations in human PIWI genes (also known as *Hiwi*), identified in individuals with azoospermia, cause cytoplasmic sequestration of RNF8 and defective H2B ubiquitylation in late spermatids and subsequent impaired histone-to-protamine exchange during spermiogenesis (Gou et al., 2017). In addition to RNF8, a number of putative ubiquitin E3 ligases have been found to be expressed during spermatogenesis (Hou et al., 2012), implying a complex histone ubiquitylation process in male germ cell development.

PHD finger protein 7 (PHF7), one of the putative testis-specific E3 ligase in humans and mice (Hou et al., 2012), has been shown to act as a conserved epigenetic reader to specifically bind histone H3 N-terminal tails with a preference for dimethyl lysine 4 (H3K4me2), and to promote male sexual determination in the *Drosophila* germline (Yang et al., 2012b). Moreover, *Phf7* (NYD-SP6 in humans) was found to be abnormally regulated in infertile males, and thus likely associated with human spermatogenesis (Xiao et al., 2002). However, the specific role of PHF7 in mammalian spermatogenesis has remained elusive. In this study, we characterized the function of PHF7 by generating *Phf7*-knockout mice using CRISPR-Cas9 technology and found that *Phf7* mutant mice exhibit male infertility due to spermatogenic failure at late spermiogenesis. Mechanistically, we found that PHF7 is a novel E3 ligase for H2A ubiquitylation, and that depletion of PHF7 results in

[1]State Key Laboratory of Cell Biology, Shanghai Key Laboratory of Molecular Andrology, CAS Center for Excellence in Molecular Cell Science, Institute of Biochemistry and Cell Biology, Chinese Academy of Science, University of Chinese Academy of Science, Shanghai 200031, China. [2]State Key Laboratory of Molecular Biology, Shanghai Key Laboratory of Molecular Andrology, CAS Center for Excellence in Molecular Cell Science, Institute of Biochemistry and Cell Biology, Chinese Academy of Science, University of Chinese Academy of Science, Shanghai 200031, China. [3]Department of Orthopaedic Surgery, Changzheng Hospital, The Second Military Medical University, Shanghai 200003, China. [4]State Key Laboratory for Conservation and Utilization of Subtropical Agro-Bioresources, Animal Reproduction Institute, Guangxi University, Nanning, Guangxi 530004, China. [5]Key Laboratory of Computational Biology, CAS-MPG Partner Institute for Computational Biology, Shanghai Institutes for Biological Sciences, Chinese Academy of Sciences, Shanghai 200031, China. [6]National Center for Protein Science Shanghai, Institute of Biochemistry and Cell Biology, Chinese Academy of Sciences, 333 Haike Road, Shanghai 201203, China. [7]CAS Center for Excellence in Molecular Cell Science, Institute of Biochemistry and Cell Biology, Chinese Academy of Science, Shanghai 200031, China. [8]Research Center of Animal Genomics, Agricultural Genomics Institute at Shengzhen, Chinese Academy of Agricultural Sciences, Shengzhen, Guangdong 518210, China.
*These authors contributed equally to this work

‡Authors for correspondence (jsli@sibcb.ac.cn; mfliu@sibcb.ac.cn; kehuanlu@163.com; erweizuo@163.com; yuanwenspine@163.com)

W.Y., 0000-0002-6394-344X; E.Z., 0000-0002-7094-0933; K.L., 0000-0002-9443-1236; M.-F.L., 0000-0003-1800-466X; J.L., 0000-0003-3456-662X

Received 9 January 2019; Accepted 28 May 2019

Development (2019) 146, dev175547. doi:10.1242/dev.175547

abnormal H2A ubiquitylation in spermatids and subsequently impairs histone-to-protamine exchange during late spermiogenesis. When the RING domain of PHF7 was inactivated, mutant mice exhibited similar male infertility phenotypes to *Phf7*-knockout mice. We further demonstrated that PHF7 plays dual roles in spermiogenesis, acting as both an epigenetic reader that can specifically bind histone H3 N-terminal tails with a preference for trimethyl lysine 4 (H3K4me3) and as an epigenetic writer that can mediate H2A ubiquitylation. Collectively, our findings indicate that PHF7 is a novel histone E3 ligase that is associated with histone-to-protamine exchange during spermiogenesis in mice.

RESULTS

PHF7 deficiency results in male infertility in mice

We first analyzed the expression profiles of *Phf7* in different tissues from adult mice. Quantitative PCR and western blot analyses indicated that *Phf7* is specifically expressed in testes. Further analyses showed that *Phf7* was highly expressed in developing sperm, but not in spermatogonial stem cells (SSCs) or Sertoli cells (Fig. S1A-D). Immunofluorescence analysis showed that PHF7 was specifically located in the nuclei of haploid spermatids (Fig. 1A). To investigate the physiological role of *Phf7* in mice, we generated *Phf7* knockout mice using CRISPR-Cas9 technology. Two sgRNAs (sg*Phf7*-A and

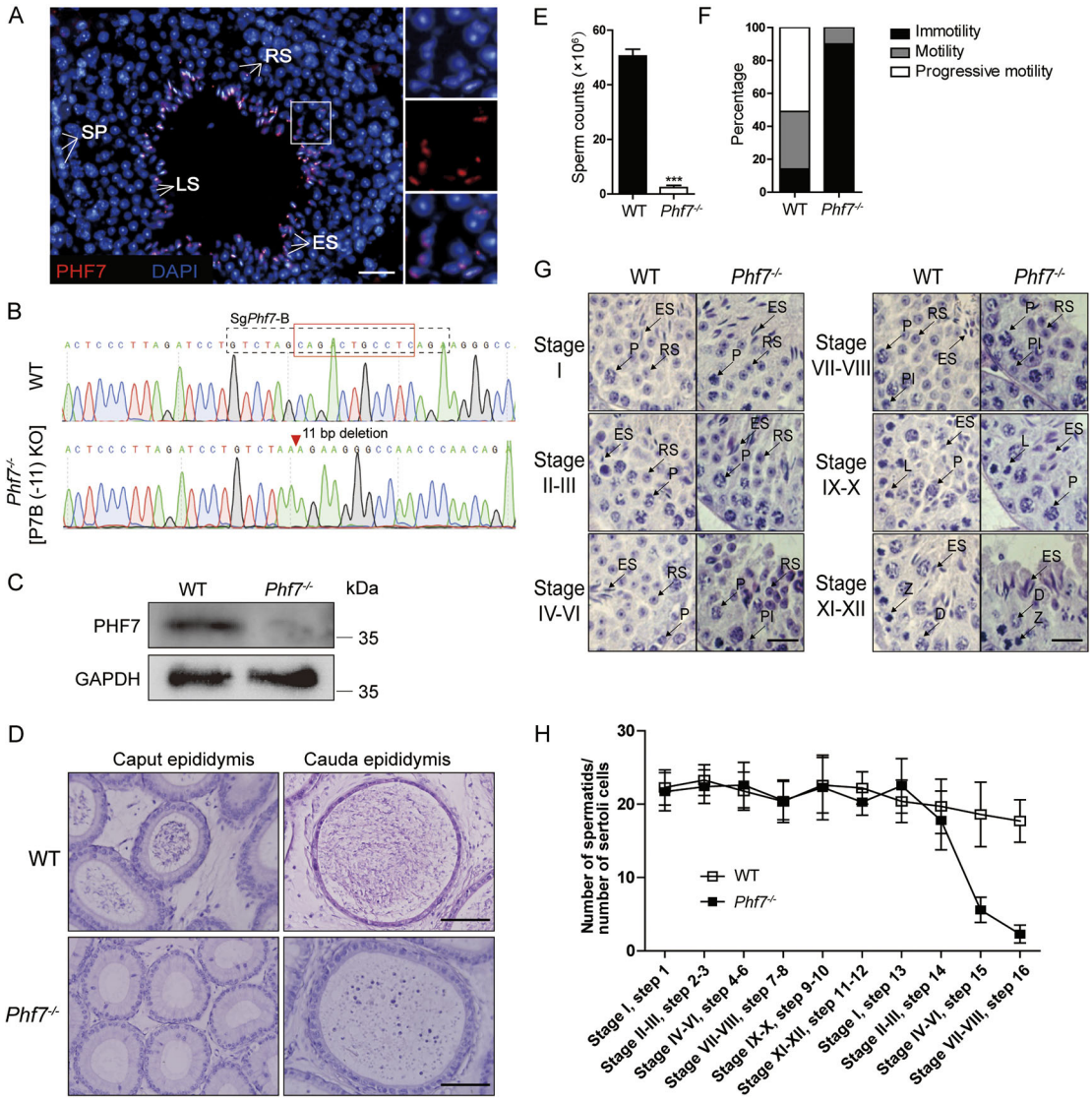

Fig. 1. *Phf7* knockout mice display male sterility. (A) Immunostaining images of testis sections from 8-week-old wild-type mice for PHF7 (red) with nuclei counterstained by DAPI (blue). Panels on right are 4× magnification of boxed area in left panel. SP, spermatocytes; RS, round spermatids; ES, elongating spermatids; LS, late spermatids. Scale bar: 50 µm. (B) Genotyping analysis of one *Phf7*$^{-/-}$ mouse line carrying an 11 bp deletion [termed P7B(-11) KO]. Black dashed box shows the sequence of sg*Phf7*-B. Red box shows the 11 bp deletion. (C) Western blot of PHF7 from the testes of mutant and wild-type 8-week-old mice. (D) Hematoxylin and Eosin staining of caput and cauda epididymis sections from 8-week-old wild-type and mutant mice. Scale bar: 50 µm. (E) Sperm counts in cauda epididymis from 8-week-old mutant and wild-type mice (n=3). Data are mean±s.d. from three separate experiments. ***P<0.001. (F) CASA assays of immotility, motility and progressive motility of sperm from 8-week-old mutant and wild-type mice. (G) Hematoxylin and Eosin staining of testis sections from 8-week-old mutant and wild-type mice. Stages of seminiferous epithelium cycles were determined by morphology of spermatocytes and round spermatids. Pl, preleptotene; L, leptotene; Z, zygotene; P, pachytene; D, diplotene; RS, round spermatids; ES, elongating spermatids. Scale bars: 20 µm. (H) Reduced number of late spermatids in *Phf7*$^{-/-}$ mice. Ratios of spermatids and Sertoli cells in tubule cross-sections of specific stages of seminiferous epithelial cycles and corresponding spermatid development steps are shown. Data are mean±s.d.

Development (2019) 146, dev175547. doi:10.1242/dev.175547

sg*Phf7*-B) were designed to target exons 2 and 4 of *Phf7*, respectively (Fig. S2A). We obtained mice with frameshift mutations via injection of Cas9 mRNA and sg*Phf7*-A or sg*Phf7*-B into zygotes with a C57BL/6 background. From these mice, females were backcrossed with wild-type (WT) males, leading to four stable mouse lines carrying mutant *Phf7* (*Phf7*$^{-/-}$), termed P7A(−1) KO, P7A(−4) KO, P7A(+1) KO and P7B(−11) KO (Fig. 1B). Knockout efficiency was confirmed using western blots (Fig. 1C). Interestingly, *Phf7*$^{-/-}$ mice were normal in growth and morphology, but males from all four lines displayed infertility (Table 1). The weights of the mutant testes and epididymes were similar to wild-type controls (Fig. S2B); however, histological analysis indicated a dramatic reduction of sperm count in mutant epididymes (Fig. 1D). Computation-assisted semen analysis (CASA) further confirmed a severe reduction of sperm count in the epididymes of *Phf7*$^{-/-}$ mice (Fig. 1E). Moreover, CASA showed little motility and forward progression of *Phf7*$^{-/-}$ sperm (Fig. 1F). These results show that *Phf7* deletion results in spermatogenic failure in male animals.

We then carefully investigated the stage at which spermatogenesis failed in *Phf7*$^{-/-}$ mice. Histological analysis of adult testes showed no obvious abnormal structure of seminiferous tubules in mutant mice (Fig. S2C). Immunostaining of testis sections for the germ cell markers MVH and γH$_2$A.X (Fig. S2D,E), the meiotic cell marker SYCP3 (Fig. S2F-G) and the acrosome marker PNA (Fig. S2H) excluded the possibilities that *Phf7* plays roles in germ cell maintenance, meiosis or early spermiogenesis. Flow analysis of DNA content of testicular cells indicated comparable ratios of 1C, 2C and 4C cells in mutant and control testes (Fig. S2I). However, histological analysis indicated that the number of elongated spermatids at step 15 and 16 (stages IV-VI, and VII-VIII) was dramatically reduced in the seminiferous tubules of *Phf7*$^{-/-}$ mice (Fig. 1G,H), concomitant with increased apoptotic signals detected in late spermatids (Fig. S2J). Taken together, these data indicate that depletion of PHF7 causes defective spermatogenesis at a later stage of spermiogenesis in mice.

To determine whether *Phf7*-deletion-induced spermiogenic defects are germ cell autonomous, we generated a mouse model carrying a *Phf7* conditional knockout allele abolishing exons 4 and 5 (referred to as *Phf7*-Loxp; Fig. S3A) using haploid embryonic stem cell (haESC)-mediated semi-cloned technology (Yang et al., 2012a; Zhong et al., 2015). We generated Sertoli cell-specific *Phf7* knockout mice [*Phf7*$^{f/-}$: *Amh*-Cre] by crossing *Phf7*-Loxp mice to a Sertoli cell-specific *Amh*-Cre transgenic mouse (Holdcraft and Braun, 2004) (Fig. S3B-D). We found that the resulting male mice exhibited normal testicular development, spermatogenesis and fertility (Fig. S3E-K), indicating that deletion of PHF7 in Sertoli cells does not impair spermatid development. In contrast, male germ cell-specific knockout mice generated by crossing *Phf7*-Loxp mice to germ cell-specific *Stra8*-Cre transgenic mice (*Phf7*$^{f/-}$: *Stra8*-Cre) (Sadate-Ngatchou et al., 2008) displayed male infertility and dramatically reduced spermatids at steps 15 and 16 (Fig. S4A-I), which resembled the phenotype observed in *Phf7*$^{-/-}$ mice. These data demonstrate that spermiogenic defects in *Phf7*$^{-/-}$ mice are most likely germ cell autonomous. We thus used *Phf7*$^{-/-}$ mice [P7B(−11) KO] for the further studies.

Table 1. Summary of the fertility test of *Phf7* knockout mice

Male	Female	Number of pups
P7A (−1) KO	Wild type	None
P7A (−4) KO	Wild type	None
P7A (+1) KO	Wild type	None
P7B (−11) KO	Wild type	None
Wild type	P7A (−1) KO	10/8/8
Wild type	P7A (−4) KO	7/9/11
Wild type	P7A (+1) KO	9/10/9
Wild type	P7B (−11) KO	8/10/9
Wild type	Wild type	10/11/9

All mutant males were infertile, whereas females were fertile.

Impaired histone-to-protamine exchange leads to reduced chromatin compaction in *Phf7*$^{-/-}$ sperm

To test whether *Phf7* deletion impairs meiosis, we examined the genome integrity of round spermatids isolated from *Phf7*$^{-/-}$ mice by round spermatid injection (ROSI) analysis (Kishigami et al., 2004; Yang et al., 2011). We found that mutant round spermatids could support offspring generation at an efficiency comparable with wild-type controls (Table S1). These results indicate that *Phf7*$^{-/-}$ mice produce haploid spermatids with genome integrity, providing additional evidence that there are no significant meiotic defects in *Phf7*$^{-/-}$ male animals. Next, we inspected the developmental potential of mutant sperm isolated from the epididymis by performing intracytoplasmic sperm injection (ICSI). The results showed that ICSI with *Phf7*$^{-/-}$ sperm induced normal activation of mature oocytes, but few injected oocytes developed into blastocysts (Table S2). Taken together, these results indicate that round spermatids from *Phf7*$^{-/-}$ mice maintain the genome integrity required to fertilize oocytes.

We then carefully analyzed the morphology of the sperm isolated from mutant epididymes. Differential interference contrast (DIC) and scanning electronic microscopy (SEM) revealed aberrant heads in the majority of mutant sperm (Fig. S5A-B, Fig. 2A), whereas PNA staining revealed normal acrosomes in mutant sperm (Fig. S5C). Transmission electron microscope (TEM) analysis further revealed less condensed nuclei in most sperm and developing spermatids from *Phf7*$^{-/-}$ epididymes and testes, respectively (Fig. 2B, Fig. S5D), suggesting defective chromatin compaction in *Phf7*$^{-/-}$ sperm.

We next investigated the potential causes of abnormal chromatin compaction in mutant sperm. Given that impaired histone-to-protamine exchange can result in less-condensed nuclei in sperm (Gou et al., 2017; Lu et al., 2010), we examined histone and protamine levels in mutant sperm. Immunostaining analysis indicated abnormal retention of H2A, H2B, H3 and H4 in *Phf7*$^{-/-}$ sperm (Fig. 2C). Western blot further confirmed increased levels of all core histones and TH2B (a testis-specific histone variant), and reduced levels of protamine PRM1 and PRM2 in *Phf7*$^{-/-}$ sperm (Fig. 2D). In elongating spermatids, where histone-to-protamine exchange has been initiated and histones are first replaced by transition proteins, we found that TNP1 (Meistrich et al., 2003; Oliva, 2006), PRM1, PRM2 and TNP1 were dramatically decreased on chromatins, while TNP1 was increased in soluble fractions in mutant mice (Fig. 2E). These results indicate impaired incorporation of transition proteins and protamines into chromatins in mutant elongating spermatids. Given the importance of histone-to-protamine exchange for chromatin compaction during spermatogenesis, these data suggest that *Phf7* deletion causes an incomplete histone-to-protamine exchange and results in defective spermiogenesis in male mice.

To reveal the mechanisms underlying abnormal histone removal, we compared the gene expression profiles of *Phf7*$^{-/-}$ round spermatids with those of wild-type round spermatids. Surprisingly, clustering analysis based on RNA-sequencing (RNA-seq) data showed a high correlation between *Phf7*$^{-/-}$ and wild-type round spermatids (Fig. 2F, Fig. S5E). The expression levels of histone-to-protamine exchange-related genes, including histones *Tnp1*, *Tnp2*, *Prm1* and *Prm2*, were similar in *Phf7*$^{-/-}$ and wild-type round

Development (2019) 146, dev175547. doi:10.1242/dev.175547

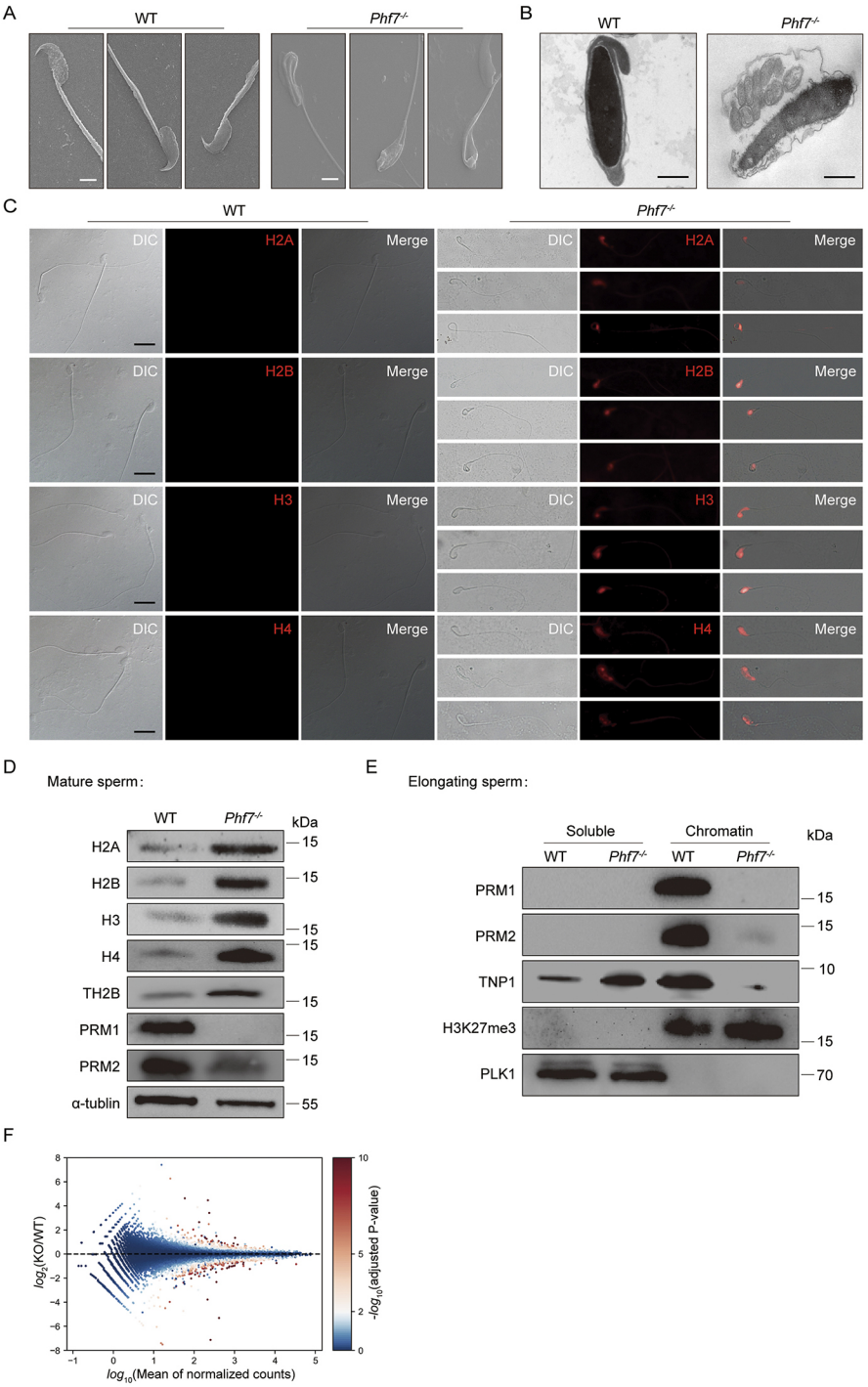

Fig. 2. Histone-to-protamine exchange is impaired during spermatogenesis in *Phf7* knockout mice. (A) Representative scanning electron microscope image of sperm from 10-week-old *Phf7* knockout (right) and wild-type (left) mice. Scale bar: 2 µm. (B) Representative transmission electron micrograph images of sperm heads from 8-week-old mutant (right) and wild-type (left) mice, showing abnormal structure of sperm heads in mutant mice. Scale bar: 2 µm. (C) Immunostaining of core histones (H2A, H2B, H3 and H4) (red) in sperm from 8-week-old *Phf7*$^{-/-}$ and wild-type males. Scale bar: 20 µm. (D) Western blot analyses of histones and protamines in mature sperm from epididymes of 12-week-old *Phf7*$^{-/-}$ and wild-type mice, with α-tubulin as a loading control. (E) Western blots of protamines and transition protein (TNP1) in soluble or chromatin-bound fractions in elongating spermatids from 8-week-old *Phf7*$^{-/-}$ and wild-type mice, with PLK1 and H3K27me3 as controls for soluble and chromatin fractions, respectively. (F) MA plot showing the differential gene expression profile between KO and wild-type mice, analyzed by DESeq2. The *y*-axis indicates the log2 fold change (KO versus wild type) of gene expression, and the *x*-axis indicates logarithmic average expression between KO and wild type. Red dots represent genes with adjusted P<0.01.

spermatids (Table 2, Fig. S5F). Taken together, these results indicate that PHF7 deficiency may not directly impede histone-to-protamine exchange through regulating gene expression, implying that PHF7 may play a role as a post-transcriptional regulator during spermiogenesis.

Table 2. Expression changes (KO versus wild type) and significance of selected genes analyzed by DESeq2

Gene	Log_2 (KO/wild type)	*P*	Adjusted *P*
Hlt	0.142	0.615	0.936
Hlt2	−0.277	0.267	0.698
Prm1	−0.167	0.634	0.938
Prm2	−0.116	0.736	0.951
Tnp1	−0.271	0.384	0.812
Tnp2	−0.261	0.409	0.830

The RING domain of PHF7 specifically ubiquitylates H2A in spermatids during the histone-to-protamine exchange process

We next asked how PHF7 regulates histone-to-protamine exchange during spermiogenesis in mice. To this end, we examined whether PHF7 physically interacts with histones by co-immunoprecipitation (co-IP) analysis. We first generated two transgenic haploid embryonic stem cell lines that stably expressed N- or C-terminal Flag-tagged PHF7 using PB-RFP-T2A-flag-Phf7 or PB-RFP-T2A-

Development (2019) 146, dev175547. doi:10.1242/dev.175547

Phf7-flag vector transfection (Fig. S6A). Flag antibody could pull down PHF7 efficiently in both cell lines (Fig. S6B-D). We detected multiple peptides of H2A and H3 using proteomic analysis of IP pellets, which are indicative of an interaction between PHF7 and histones (Fig. S6E).

Previous studies have demonstrated that PHF7 contains the RING domain (Hou et al., 2012; Wei et al., 2017), an E3 ubiquitin ligase signature (Deshaies and Joazeiro, 2009). Ubiquitylation of H2A/H2B in elongating spermatids is an early step in histone-to-protamine exchange (Gou et al., 2017; Lu et al., 2010; Rathke et al., 2014), so we next examined the levels of ubiquitylated H2A and H2B in spermatids isolated from *Phf7*$^{-/-}$ testes. Western blotting revealed dramatically decreased ubiquitylation of H2A (ub-H2A), but not H2B in mutant spermatids relative to wild-type controls (Fig. 3A). Immunostaining of spermatids at different stages showed a significant reduction of ub-H2A in the nuclei of round spermatids (Fig. 3B). In contrast, the levels of ub-H2B and H4K16Ac, an event downstream of ub-H2B (Lu et al., 2010), were not changed in mutant spermatids (Fig. S6F,G). Taken together, these data suggest that H2A, not H2B, is the ubiquitylation target of PHF7.

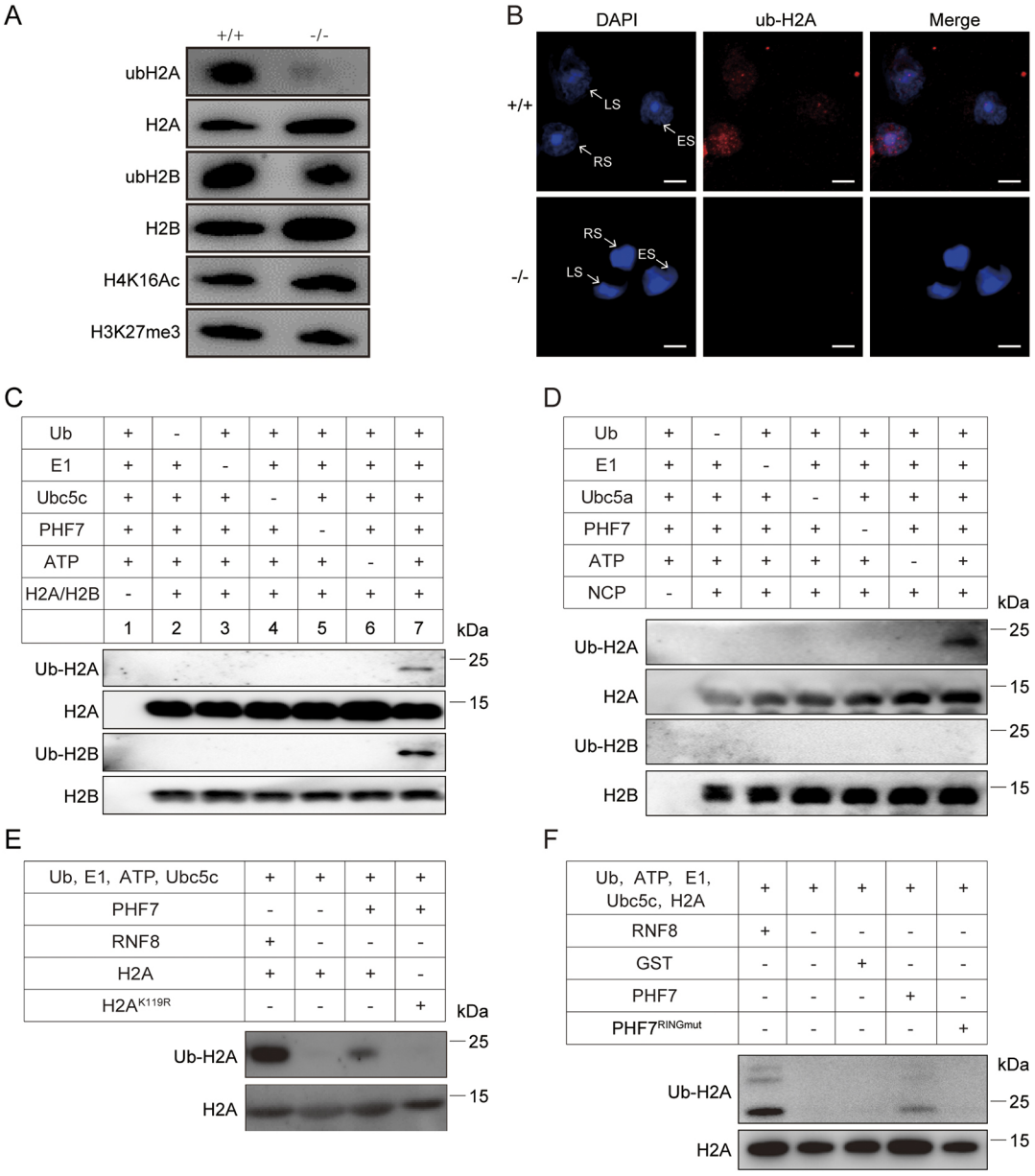

Fig. 3. PHF7 as a spermiogenesis-specific E3 ligase can ubiquitylate histone H2A *in vitro*. (A) Western blot of ub-H2A, ub-H2B and H4K16Ac in spermatids from 8-week-old mice, with H3K27me3 serving as a loading control. (B) Immunostaining of ub-H2A (red) at different stages in spermatids isolated from 8-week-old mice. Nuclei are stained with DAPI (blue). RS, round spermatids; ES, elongating spermatids; LS, late spermatids. Scale bar: 10 µm. (C) *In vitro* ubiquitylation analysis showing that PHF7 could ubiquitylate H2A and H2B. (D) *In vitro* ubiquitylation analyses showing that PHF7 could only ubiquitylate histone H2A of nucleosome core particles (NCPs). (E) PHF7 protein could not ubiquitylate H2A carrying K119R (H2AK119R), the common ubiquitylation site of H2A *in vitro*. RNF8 served as a positive control E3 ligase. The PHF7 and RNF8 proteins were purified from *E. coli* expressing pET-51b-PHF7/RNF8 plasmid. (F) GST-PHF7 protein carrying a mutation in the conserved motif of the RING domain (Cys3-His-Cys4 mutated to Ala3-Ala-Ala4, termed as PHF7^{RINGmut}) could not ubiquitylate histone H2A *in vitro*. PHF7 and PHF7^{RINGmut} proteins were purified from *E. coli* expressing the pGEX6P-1-PHF7/PHF7^{RINGmut} plasmid. RNF8 and GST served as positive and negative controls, respectively.

Development (2019) 146, dev175547. doi:10.1242/dev.175547

To directly test the role of PHF7 in histone ubiquitylation, we established an *in vitro* PHF7 ubiquitylation assay using H2A or H2B as substrates. H2A could be consistently mono-ubiquitylated by purified PHF7 *in vitro*. Interestingly, in contrast with *in vivo* observations, PHF7 could also mono-ubiquitylate H2B *in vitro* (Fig. 3C). The potential explanation might be that the core histones (H2A, H2B, H3 and H4) constitute nucleosomes *in vivo*, which interact with PHF7, leading to different ubiquitylation outcomes compared with the *in vitro* assay, wherein a single core histone was used as a substrate. To further investigate this possibility, we constituted nucleosome core particles (NCPs) and subjected them to *in vitro* ubiquitylation assays, as described previously (Leung et al., 2014). As expected, PHF7 could only ubiquitylate H2A of NCPs *in vitro* (Fig. 3D). C-terminal K119 is the common ubiquitylation site of H2A (Huen et al., 2007; Kouzarides, 2007), so we reconstituted and purified H2A with mutant K119 for *in vitro* analysis. We found that PHF7 could not ubiquitylate mutant H2A (Fig. 3E). Finally, purified PHF7 with a mutant RING domain could not ubiquitylate H2A *in vitro* either (Fig. 3F). Taken together, these data demonstrate that H2A is the substrate of the PHF7 E3 ligase during spermiogenesis.

To directly test the relationship between PHF7 and H2A ubiquitylation in mice, we generated mice carrying *Phf7* with a mutant RING domain (*Phf7*^{RINGmut}) (Fig. 4A, Fig. S7A) and western blot analysis revealed comparable expression of PHF7 in *Phf7*^{RINGmut} spermatids and wild-type spermatids (Fig. S7B). As expected, the mutant mice exhibited similar infertility phenotypes to *Phf7*$^{-/-}$ mice (Fig. 4B-E, Fig. S7C,D). Consistent with the above *in vitro* results with PHF7^{RINGmut} (Fig. 3F), ub-H2A was almost undetectable in round spermatids from *Phf7*^{RINGmut} males (Fig. 4F,G, Fig. S7E,F). Taken together, these data demonstrate that PHF7 is a novel E3 ligase that ubiquitylates H2A via its RING domain in round spermatids during spermiogenesis.

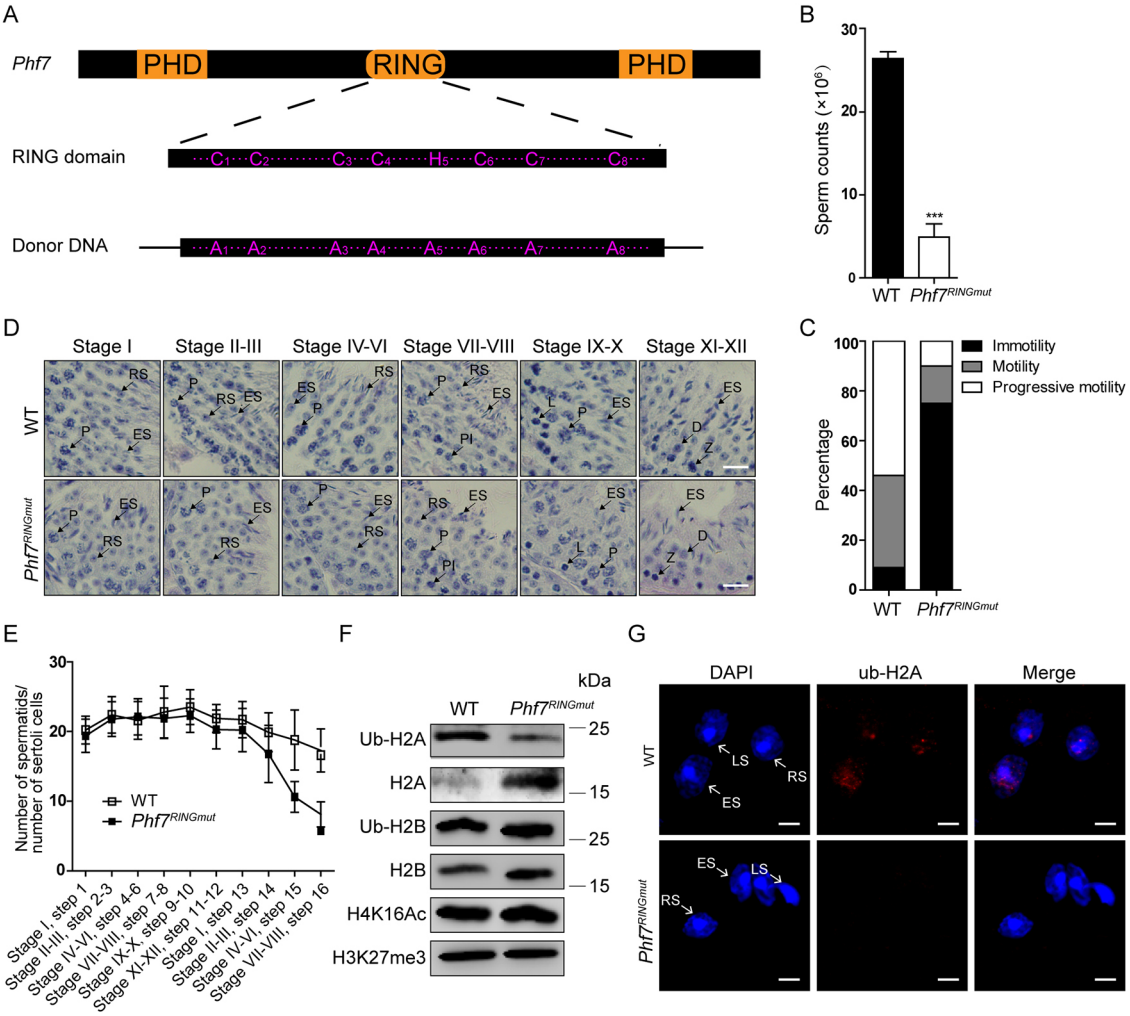

Fig. 4. The RING domain of PHF7 specifically ubiquitylates histone H2A in spermatids. (A) A schematic illustrating the donor DNA used for generation of mice carrying mutant *Phf7* RING domain. The yellow modules represent functional domains of PHF7. All Cys and His in the conserved motif (C4HC3) of the RING domain were mutated to Ala. (B) Sperm counts in cauda epididymis from 8-week-old mouse carrying mutant RING domain (*Phf7*^{RINGmut}). Data are mean±s.d. from three separate experiments ***P<0.001. (C) CASA assays of immotility, motility and progressive motility of sperm from 8-week-old *Phf7*^{RINGmut} mice. (D) Hematoxylin and Eosin staining of testis sections from 8-week-old *Phf7*^{RINGmut} mice. Stages of seminiferous epithelium cycles were determined by the morphology of spermatocytes and round spermatids. PI, preleptotene; L, leptotene; Z, zygotene; P, pachytene; D, diplotene; RS, round spermatids; ES, elongating spermatids. Scale bars: 20 µm. (E) A reduced number of late spermatids was observed in *Phf7*^{RINGmut} mice. Ratios of spermatids and Sertoli cells in tubule cross-sections of specific stages of seminiferous epithelial cycles and corresponding spermatid development steps are shown. (F) Western blot of ub-H2A, ub-H2B and H4K16Ac in haploid spermatids from 8-week-old *Phf7*^{RINGmut} and wild-type mice, with H3K27me3 serving as a loading control. (G) Ub-H2A (red) immunostaining in different stages of spermatids isolated from 8-week-old *Phf7*^{RINGmut} mice. Nuclei were stained with DAPI (blue). RS, round spermatids; ES, elongating spermatids; LS, late spermatids. Scale bars: 10 µm.

Development (2019) 146, dev175547. doi:10.1242/dev.175547

PHF7 links H3K4 methylation to H2A ubiquitylation through its PHD domains during spermiogenesis

A previous study indicated that the PHD domain of PHF7 binds histone H3 N-terminal tails with a preference for dimethyl lysine 4 (H3K4me2) and controls *Drosophila* male sex determination (Yang et al., 2012b). This information, coupled with our proteomic analysis of IP pellets showing direct interaction between PHF7 and H3 (Fig. S6E), led us to hypothesize that PHF7 might be an epigenetic reader that recognizes H3 modifications during spermiogenesis in mice.

To test this hypothesis, we first examined whether PHF7 functionally interacts with H3. Indeed, at least five independent pieces of evidence indicated a functional link between PHF7 and H3. First, glutathione S-transferase (GST) pull-down assays (Shechter et al., 2007; Shi et al., 2006) showed a direct interaction between PHF7 and histones (Fig. 5A), and western blot analyses of GST-PHF7-bound histones revealed significant enrichment of H3 (Fig. 5B). Second, we checked which modifications could be recognized by PHF7 and identified that H3K4 modifications, including H3K4me2 and H3K4me3, were PHF7-binding sites (Fig. 5C). Third, in far-western blot analyses (Wu et al., 2007), PHF7 strongly bound H3K4me3, with lower affinity for H3K4me2 (Fig. 5D). Fourth, we tested the recognition of methylated H3K4 by PHF7 in the context of physiological chromatin in cells using protein-protein chromatin immunoprecipitation (ChIP) assays (Ricke and Bielinsky, 2005). As expected, the results further confirmed that PHF7 was strongly associated with H3K4me3 and H3K4me2 (Fig. 5E). Fifth, purified PHF7 with mutant PHD domains could not bind H3K4me3 and H3K4me2 *in vitro* (Fig. 5F). Taken together, these data indicate that PHF7 specifically binds with H3K4me3 and H3K4me2.

Having demonstrated that RING domain-containing PHF7 can ubiquitylate H2A, and that its PHD domain can recognize H3K4 methylation, we next investigated the functional connection between PHD and the RING domain by performing chromatin immunoprecipitation sequencing (ChIP-seq) using antibodies against PHF7, H3K4me3 and ub-H2A. To this end, we generated a *Phf7*-Flag knock-in mouse line (*Phf7*-KI-Flag) by injection of haESCs carrying a *Phf7*-Flag knock-in into oocytes (Zhong et al., 2015) (Fig. S8A). Western blot and co-IP analyses showed that the anti-FLAG antibody could faithfully and efficiently recognize and pull down PHF7 in round and elongating spermatids (Fig. S8B,C). ChIP-seq analysis of spermatids isolated from the testes of *Phf7*-KI-Flag mice according to a previously reported protocol (Bastos et al.,

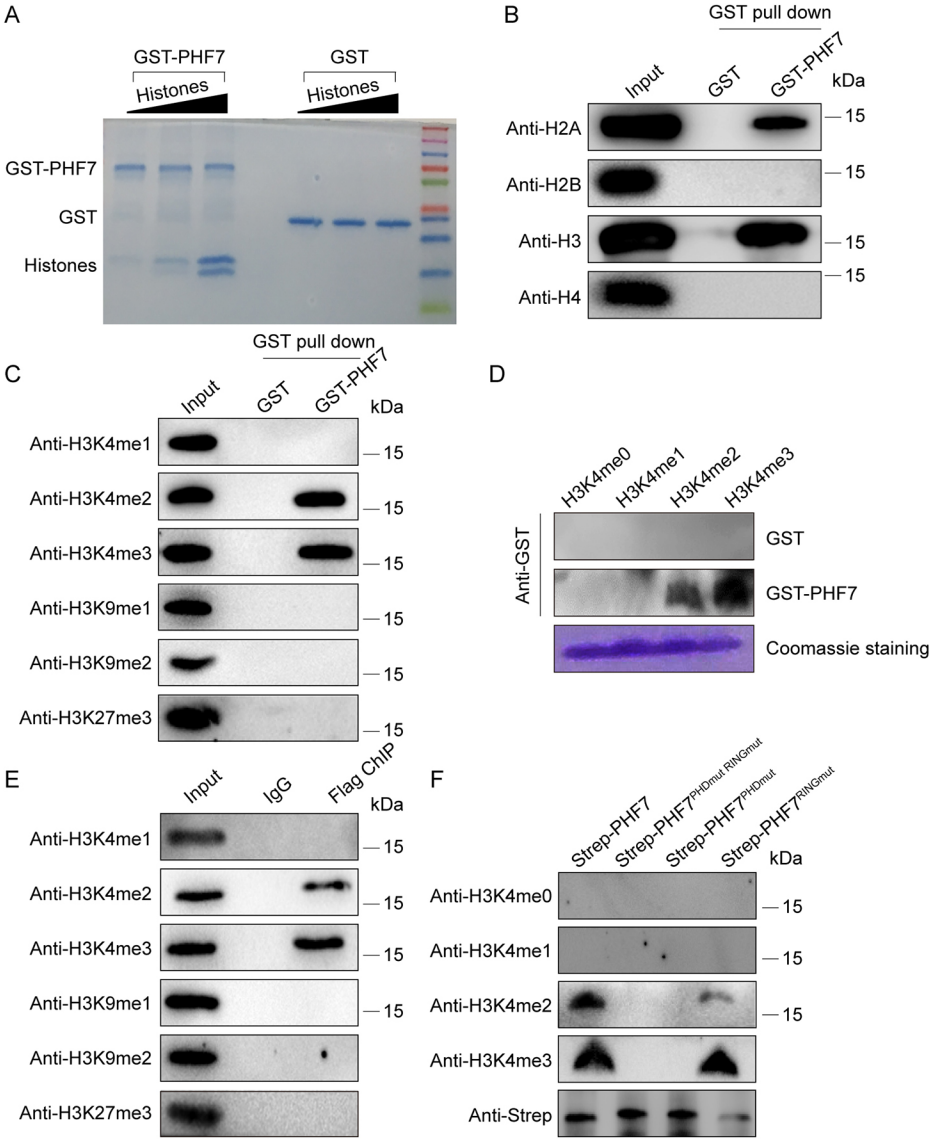

Fig. 5. The PHD domain of PHF7 prefers to bind H3K4me3 modification. (A) Coomassie Blue staining of glutathione S-transferase (GST)-PHF7 and GST control pulldown from bulk histones, showing the direct interaction between GST-PHF7 and extracted bulk histones. (B) Western blot analysis of GST-PHF7-bound histones using antibodies against H2A, H2B, H3 and H4. The input load represents 10% of total histones. (C) Western blot analysis of GST-PHF7-bound histones using antibodies against histone H3 methylation modifications. The input load represents 10% of total histones. (D) Far western blot showing direct binding of GST-PHF7 with H3K4me3/me2 *in vitro*. Histone peptides, including H3K4me0, H3K4me1, H3K4me2 and H3K4me3, were used for analysis. The same amount of peptides served as the loading control for Coomassie Blue staining. (E) Protein-protein ChIP assay showing a strong interaction between PHF7 and H3K4me3/H3K4me2 *in vivo*. Western blot analysis of Flag-PHF7 protein-protein ChIP is shown. The input load represents 10% of total histones. (F) Strep-PHF7 carrying a mutant PHD domain could not bind H3K4me3/me2. Strep-PHF7$^{PHDmut\ RINGmut}$ is a PHF7 protein carrying both mutant RING (Cys3-His-Cys4 mutated Ala3-Ala-Ala4) and PHD (Cys4-His-Cys3 mutated to Ala4-Ala-Ala3) domains in its conserved motif. Strep-PHF7^{PHDmut} is a PHF7 with mutant PHD domain. Strep-PHF7^{RINGmut} is a PHF7 protein with mutant RING domain.

Development (2019) 146, dev175547. doi:10.1242/dev.175547

2005) showed that the binding peaks of PHF7 and H3K4me3 were mainly enriched at the promoter (Fig. 6A). More than 96% (n=15,419) of all PHF7-binding peaks overlapped with those of H3K4me3 (Fig. 6B), providing supporting evidence for the specific binding of PHF7 to H3K4me3. Moreover, the common binding genes between PHF7 and H3K4me3 were associated with ub-H2A (Fig. 6C,D, Fig. S8D).

However, we observed even lower ub-H2A levels in the immediate vicinity of the TSSs of PHF7-binding genes compared with PHF7 non-binding genes (data not shown), suggesting that other E3 ligases might be involved in the process of binding and ubiquitylating PHF7 nonbinding genes. In future studies, it will be interesting to identify which histone E3 ligase is responsible for histone ubiquitylation in PHF7 nonbinding genes. Finally, H3K4me3 unique genes exhibited higher ub-H2A levels, implying that H3K4me3 could be one of the marks for H2A ubiquitylation during spermiogenesis (Fig. 6D). Taken together, these results demonstrate that PHF7 ubiquitylates H2A, likely by binding H3K4me3.

DISCUSSION

Ubiquitylation of histones is crucial prior to histone-to-protamine exchange during spermiogenesis. High-throughput analyses identified many factors that may be involved in this process (Hou et al., 2012). Of these factors, only RNF8 has been demonstrated to ubiquitylate core histones, especially H2B, in elongating spermatids (Gou et al., 2017; Lu et al., 2010). In this study, we demonstrate that PHF7 is a novel E3 ligase, which can specifically ubiquitylate H2A in round spermatids. PHF7 deletion results in reduced ub-H2A in round spermatids, retention of histones in sperm and male infertility. Moreover, we demonstrated that the RING domain of PHF7 ubiquitylates H2A, probably through binding H3K4me3 and H3K4me2 by its PHD domains.

Previous studies have shown that PHF7 is a histone code reader, which can specifically associate with H3K4me2/me3 and determine sex in *Drosophila* (Yang et al., 2012b). However, how PHF7 affects chromatin structure is still an unresolved issue. Our observations in mice further confirm that the PHD finger domain of PHF7, as the most conserved domain between *Drosophila* and mammals (Yang et al., 2012b), acts as the histone code reader to specifically bind H3K4me2/me3. Interestingly, *Drosophila* PHF7 associates preferentially with H3K4me2 over H3K4me3, whereas mouse PHF7 acts preferentially with H3K4me3 over H3K4me2, consistent with previous reports of the human ING2 PHD domain (Shi et al., 2006). Moreover, our results reveal that the RING domain of mouse PHF7 can also act as an epigenetic writer to ubiquitylate H2A in round spermatids, which is associated with histone-to-protamine exchange. Several pieces of

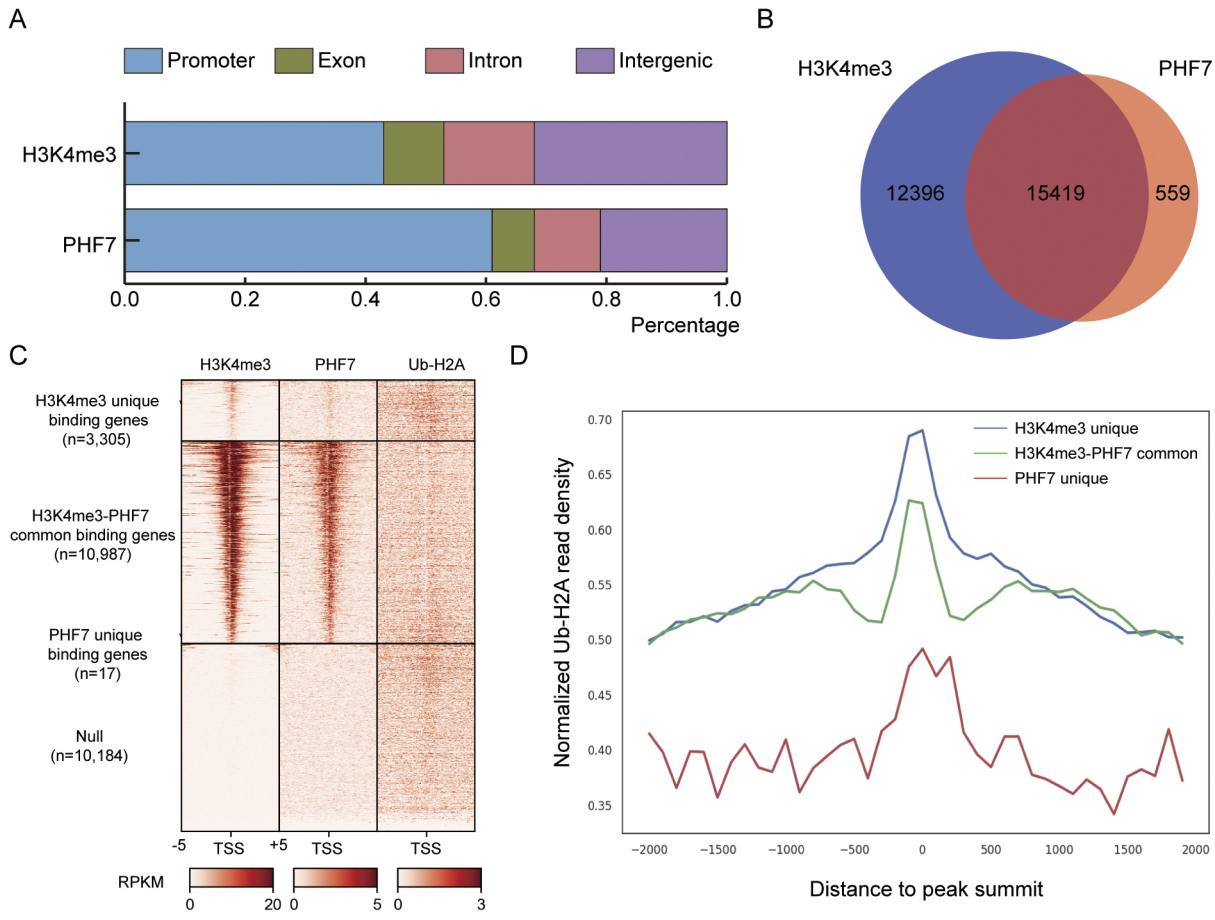

Fig. 6. PHF7 links H3K4 methylation to H2A ubiquitylation during spermiogenesis. (A) Distribution of binding peaks of PHF7 and H3K4me3 in different genomic regions. The binding peaks across the mouse genome were classified into four genomic locations categories, including exon, promoter and intergenic regions. Peak distribution was plotted according to the percentage of total peaks. (B) Venn diagram showing the number of gene promoters bound by PHF7 and H3K4me3, as identified by ChIP-seq, demonstrating colocalization of H3K4me3 with PHF7 within promotors. (C) A heatmap showing the distribution of binding peaks of PHF7, H3K4me3 and ubH2A in spermatids. Density around islands (±5 kb from the center of islands) is shown. (D) Signal of ub-H2A read density in different modules. The plotted curves are the average profiles of H3K4me3 unique, H3K4me3-PHF7 common and PHF7 unique read coverage distanced to peak summit in a 4000 bp window of all RefSeq genes.

Development (2019) 146, dev175547. doi:10.1242/dev.175547

evidences from co-IP, GST pull-down and protein ChIP strongly demonstrate that PHF7 can simultaneously recognize and bind both H2A and H3. Moreover, ChIP-seq experiments indicate that PHF7 specifically binds H3K4me3 *in vivo*, which associates with ub-H2A. These observations suggest that it is most likely that *Phf7* acts as E3 ligase to ubiquitylate H2A by specifically binding H3K4me3 during spermatid maturation.

A large number of studies have shown that the correct dose of protamine is essential for genome compaction and formation of functional sperm (Cho et al., 2003, 2001). Interestingly, in this study, both $Phf7^{-/-}$ and $Phf7^{RINGmut}$ mice exhibited reduced levels of protamine in elongating spermatids and mature sperm (Fig. 3E,F, Fig. S7C,D). Together with evidence that PHF7 can specifically bind with H3K4me3/2 (an important marker for transcription in spermatogenic cells) in round spermatids (Siklenka et al., 2015), these observations imply that PHF7 may also act as a transcriptional regulator during spermiogenesis. However, RNA-seq and qPCR analyses showed that $Phf7^{-/-}$ round spermatids exhibited a similar expression profile to wild-type controls, and that all tested histone-to-protamine exchange-related genes were similarly expressed in mutant and wild-type round spermatids (Fig. 2F, Fig. S5E,F, Table 2). In addition, given the nuclear location of PHF7 protein in mouse spermatids (Fig. 1A, Fig. S9A), it is less likely that PHF7 is directly involved in regulating the translation of protamine mRNAs. Additionally, we found that PHF7 binding peaks were not enriched in the promoters of histone-to-protamine exchange-related genes. Taken together, our results may exclude the possibility that PHF7 regulates the histone-to-protamine exchange through controlling the transcription of related genes. We thus speculate that the reduction of protamine proteins in $Phf7^{-/-}$ spermatids is likely due to an indirect effect on translation and/or stability of protamine proteins during spermiogenesis. Future studies will be needed to understand the link between PHF7-mediated H2A ubiquitylation and histone-to-protamine exchange in the future.

Although previous data have shown that RNF8 is involved in the histone-to-protamine exchange process during spermiogenesis, the topic remains controversial (Lu et al., 2010; Sin et al., 2012). Our data demonstrate that PHF7 plays a crucial role in this process. However, exactly how PHF7 cooperates with RNF8 during the histone-to-protamine exchange process remains unclear. Our studies imply an orchestrated sequence of histone ubiquitylation by PHF7 and RNF8 during spermiogenesis. Our evidence suggests that PHF7 may begin ubiquitylation of H2A in round spermatids, followed by RNF8-induced ubiquitylation of H2A and H2B, with a preference for H2B in elongating spermatids. We therefore propose that histone ubiquitylation, a crucial step prior to histone-to-protamine exchange, is regulated by PHF7 and RNF8 sequentially during spermiogenesis. This work deepens our knowledge of the epigenetic regulation underlying histone-to-protamine exchange during spermiogenesis. However, future studies will be needed to understand the molecular mechanisms underlying PHF7 and RNF8 mediated histone ubiquitylation, and their link to histone-to-protamine exchange.

MATERIALS AND METHODS

Animal use and care

All animal procedures were approved under the ethical guidelines of the Institute of Biochemistry and Cell Biology, Chinese Academy of Sciences.

RNA extraction and RT-PCR

Forceps were used to isolate different tissue samples from mice, which were placed in the corresponding Trizol tube. The samples were fully homogenized to extract high-quality RNA for reverse transcription followed by a Trizol-guided protocol. 1 µg RNA was first reverse transcribed into cDNA using the reverse transcriptase Rever Tra Ace qPCR RT Master Mix with gDNA Remover (Toyobo, FSQ-201) according to the manufacturer's instructions and the resulting cDNA was used as a template for subsequent PCR amplification using primers specific for one or more genes.

Isolation of mouse spermatogenic cells

Mouse Sertoli, Leydig and spermatogenic cells were isolated from testes as previously described (Chang et al., 2011; Zhang et al., 2014). Briefly, mouse testes were harvested and the tunica albuginea was removed to expose the seminiferous tubules using surgical scissors. The testes were then cut into pieces and incubated in 3 ml collagenase type IV at 37°C for 15 min. After incubation, the tissue was resuspended with 3 ml of Trypsin for 10 min. After neutralization of the Trypsin with an equal volume of DMEM/10% FBS, the mixture was filtered with a 70 µm filter. The spermatogenic cell suspension was stained with Hoechst 33342 (5 µg/ml, Thermo Fisher Scientific, H1399) for 15-30 min at 37°C, and sorted according to DNA content and forward scatter parameter (FSC) (Bastos et al., 2005). The two types of spermatids exhibit distinguished FSC, which allows separation into two subpopulations. The FSC^{high} and FSC^{low} populations represent round spermatids and elongated spermatids, respectively. Isolated spermatogenic cells were confirmed by their distinct nuclear morphology (using DAPI staining of nuclei).

Sperm isolation and CASA analysis

Sperm were harvested by dissecting the cauda epididymis in 37°C pre-warmed Eagle's medium (Sigma, D6046) supplemented with 25 mM HEPES and 4 mg/ml bovine serum albumin (BSA). Blood vessels were dissected away to prevent blood cell contamination of spermatozoa, and epididymis was washed in Ham's F10 medium (Sigma, N2147) containing 4 mg/ml BSA. Spermatozoa were released into 1 ml of Ham's F10 through puncture cut by scissors, gently filtered on ice through fine nylon mesh to remove tissue debris, and harvested by spinning at 500 ***g*** for 10 min at 4°C. Sperm-containing medium was dropped into a calibrated slide for CASA analysis. Accurate assessment of motion parameters for each species is dependent upon the computer settings and the concentration of spermatozoa analyzed, so each calibration parameter of the Cell Track/s System was optimized to track felid spermatozoa by evaluating prerecorded samples at various settings.

GST-tagged or strep-tagged protein purification

Plasmids used for expression of different proteins were constructed in the backbone of pGEX6P-1 or pET-51b. The procedures of GST-tagged or Strep-tagged protein purification were carried out according to the manufacturer's instructions (IBA, Manual Strep-Tactin Purification; Millipore, Protein purification and preparation). All primer sequences are listed in Table S3.

Immunostaining analysis

Cells on glass and tissue sections were fixed with 4% PFA in PBS for 15 min at room temperature, followed by washing three times every 5 min with PBS. The samples were then blocked with permeabilizing buffer (10% FBS, 1% BSA, 1% Triton X-100, 88% PBS) for 1-2 h. All primary antibodies (Table S3) were diluted (if not specified, the antibody dilution ratio is 1:1000) by blocking buffer (10% FBS, 1% BSA, 89% PBS) and incubated with samples overnight at 4°C, followed by washing with PBS three times every 5 min. The samples were treated with secondary antibody (if not specified, the antibody dilution ratio is 1:1000) coupled with fluorescence for another 1 h at room temperature. Nuclei were stained with DAPI for 10 min. Laser confocal scanning images were captured with a Leica TCS SP5 inverted spectral confocal microscope. Immunostaining density was quantified using ImageJ software.

Immunoprecipitation and immunoblot

Mouse spermatogenic cells or other cells were lysed in the buffer [50 mM Tris-HCl (pH 7.4), 1% Triton X-100, 0.1% NP-40, 150 mM NaCl, 5 mM EDTA, 1× proteinase Inhibitor cocktail (Roche, 4693159001)]. Primary antibody-coupled Protein G beads (Life Technologies, REF10004D) were added to the precleared cell lysate and incubated for 4-6 h at 4°C. After washing the Protein G beads with the washing buffer [50 mM Tris-HCl (pH 7.4), 0.1% Triton X-100, 500 mM NaCl, 5 mM EDTA, proteinase inhibitor

Development (2019) 146, dev175547. doi:10.1242/dev.175547

cocktail] three times, the IP pellets and extracts of cells were analyzed by standard SDS-PAGE and IB procedures.

ROSI, ICSI and ICAHCI

MII-arrested oocytes were collected from 8-week-old superovulated B6D2F1 females and cumulus cells were removed using hyaluronidase. For ROSI, round spermatids were enriched from testicular cell suspension pretreated with Hoechst 33342 by FACS and injected into oocytes in HEPES-CZB medium containing cytochalasin B (CB, 5 µg/ml). The injected oocytes were activated by treatment with $SrCl_2$ for 6 h and then cultured in KSOM medium at 37°C under 5% CO_2 in air (Wu et al., 2015). For ICSI, mature sperm collected from the epididymis were injected into oocytes according to reported protocols (Kishigami et al., 2004; Yang et al., 2011). For ICAHCI, haploid ESCs were used in place of round spermatids for injection. The injected oocytes were cultured for 24 h or 3.5 days to reach the two-cell embryo or blastocyst stage for transplantation into the oviducts or uteri of pseudopregnant ICR females, respectively (Zhong et al., 2015).

In vitro ubiquitylation assays

In vitro ubiquitylation assays were performed as previously described (Gou et al., 2017). The ubiquitylation reaction mixture contained 50 mM (pH 7.5) Tris, 5 mM $MgCl_2$, 2 mM NaF, 2 mM ATP, 10 mM okadaic acid, 1 mM DTT, 0.1 mg E1, 0.2 mg UbcH5c or UbcH5a and 1 mg HA-ubiquitin (all from Boston Biochemisty). Histones (New England Biolabs, 1 µg) or nucleosome core particles (4 µg) were incubated in 30 µl ubiquitylation reaction buffer, and purified GST-PHF7 or RNF8 was added to the mixture for 2-4 h at 37°C. The proper amount of SDS loading buffer was then added to terminate the reaction before running an SDS-PAGE gel.

GST pull-down

GST beads (10 µl beads/sample, GE Healthcare Life Sciences, 17513201) were washed three times every 5 min with PBS. Purified GST and GST-PHF proteins were incubated with GST beads overnight at 4°C and rotated gently. The bead-protein complexes were collected via centrifugation for 2 min at 1500 ***g*** at 4°C and washed three times with PBS. The bead-protein complexes were mixed with extracted histones and incubated for another 4-6 h at 4°C. After centrifugation (1500 ***g*** for 2 min at 4°C), the bead-protein-histone complexes were collected and washed three times before being subjected to SDS-PAGE analysis.

Far-western blotting

Far-western blotting used a non-antibody protein that is known to bind the protein of interest. Commercial histone peptides (H3, H3K4me1, H3K4me2 and H3K4me3) were separated using 20% native PAGE gel and were then transferred to a 0.1 µm nitrocellulose filter membrane (GE Healthcare Life Sciences, 10600000). The membrane was incubated with 2% BSA for 3 h at room temperature. For the purified protein GST-PHF, the membrane was incubated overnight at 4°C (GST protein was used as a negative control). After incubation, the membrane was washed gently in PBS before being incubated with GST antibody. Next, the secondary HRP-conjugated antibody was used to detect the protein bound to the histone peptides.

Protein-protein ChIP

Our protein-protein ChIP protocol was modified from the paper published in 2005 (Ricke and Bielinsky, 2005). Specifically, cells constitutively expressing Flag-tagged PHF7 were crosslinked with 10 ml PBS containing 1% formaldehyde (freshly prepared by mixing 270 µl of 37% formaldehyde into 10 ml PBS) at room temperature for 10 min. A 1/20 volume of 2.5 M glycine was added to a final concentration of 0.125 M to quench the formaldehyde and mixed gently on a rocking station for 10 min. Cell pellets were collected and suspended in lysis buffer [0.5% NP-40, 10 mM EDTA, 50 mM (pH 8.0) Tris-HCl]. Chromatin was sonicated using a Bioruptor PLUS (Pico, 15 cycles, 15 s on/90 s off). After centrifugation at 13,400 ***g***, Protein G beads were used to preclear the lysate. The sonicated chromatin was then incubated with Flag antibody, followed by Protein G beads. IgG was used as a negative control. Last, the binding complex was eluted with elution buffer (0.1 mM $NaHCO_3$, 1% SDS) and the formaldehyde crosslink reversed before detection of histone modifications.

RNA-seq and functional enrichment analysis

We isolated round spermatids from the testes of wild-type and *Phf7* knockout mice, according to a previously reported protocol (Bastos et al., 2005) for downstream analysis. Round spermatids mRNA profiles from 8-week-old wild-type and *Phf7* knockout mice were generated by deep sequencing, in triplicate, using an Illumina HiSeq X10. Illumina Casava1.7 software was used for basecalling. RNA-seq reads were trimmed for adapter sequence using trim-galore v0.5.0, then mapped to mm9 with STAR v2.6.0. Raw read counts of mm9 RefSeq annotated genes were generated by feature Counts v1.5.3 with parameters -p -C, and only uniquely mapped reads were counted. Differentially expressed genes were analyzed by DESeq2 with default parameters. Genes with log2 fold change above 1 (upregulated in the KO) or below −1 (downregulated in the KO) and an adjusted $P<0.05$ were identified as differential expressed genes. Track files were generated using bedtools genomecov v2.27.1 with -split and then converted to bigwig format with bedGraphToBigWig. The values in bigwig files represent the raw read coverage without any normalization.

ChIP-seq and data processing

Haploid spermatids were isolated from the testes of 8-week-old males as described above. Spermatids were fixed in 1% formaldehyde at room temperature for 10 min and neutralized in 0.125 M glycine for 10 min at a rocking station, followed by cytoplasm cell lysis [10 mM Tris-HCl (pH 8), 10 mM NaCl, 0.5% NP-40, 1×protease inhibitor cocktail] on ice for 10 min, then nuclear lysis buffer [1% SDS, 10 mM EDTA, 50 mM Tris-Cl (pH 8.1), 1× protease inhibitor cocktail] on ice for 10 min. Samples were diluted in 20 mM Tris-HCl (pH 8), 2 mM EDTA, 150 mM NaCl, 0.01% SDS and 1% Triton X-100, and then sonicated using a Bioruptor PLUS (12 cycles, 30 s on/30 s off). The whole-cell extract was precleared with 50 µl protein G beads. After centrifugation at 1500 ***g***, the supernatant was incubated overnight at 4°C with 30 µl of Protein G agarose beads and 5 µg of the appropriate antibodies. Beads were washed four times with ChIP buffer and once with TE buffer. Bound complexes were eluted from the beads and crosslinking was reversed by overnight incubation at 65°C. Immunoprecipitated DNA and whole-cell extract DNA (input sample) were then purified using Qiagen PCR purification kit (Qiagen, 28104). The ChIP-seq library was constructed using NEBNext Ultra DNA Library Prep Kit for Illumina (NEB, E7370). By obtaining over 20 M sequences from every sample according to the standard pipeline for chromatin immunoprecipitated DNA (Landt et al., 2012; Rozowsky et al., 2009), we generated genome-wide chromatin-state maps and mapped the PHF7 binding position of late spermatids. Every sample had one replicate and the ChIP-seq analysis was performed as followed: first basecalls were performed using CASAVA version 1.4, then ChIP-seq reads were aligned to the mm9 genome assembly using Bowtie version 1.2 (with configurations -m 1 -X 500). Only uniquely aligned reads were kept for downstream analysis. Peaks were called using MACS 1.3.7.1 with default parameters. Finally, signal tracks were generated using this pipeline, and the fold-change track was used for further analysis.

Acknowledgements

We thank Linyu Lu for *Rnf8*-deficient mice and Ronggui Hu from SIBCB for discussion. We also thank Dr Qinghua Shi from USTC for providing related genetic information on male infertility in humans.

Competing interests

The authors declare no competing or financial interests.

Author contributions

Conceptualization: X.W., E.Z., J.Li, M.-F.L.; Methodology: X.W., J.-Y.K., L.W., H.S., S.Y., L.L., M.Y., M.B., Y.C., J. Long; Software: X.W.; Validation: X.W., J.-Y.K.; Formal analysis: X.W., J.K., L.W., X.Y., H.S., S.Y., L.L., M.Y., M.B., Y.C., J. Long, Z.S.; Investigation: X.W., L.W.; Resources: X.W., J.-Y.K., L.W.; Data curation: X.W.; Writing - review & editing: J. Li, M.-F.L., N.L., D.L., J.H., M.L., Z.S.; Visualization: J. Li, K.L., E.Z., W.Y.; Supervision: J. Li, W.Y., X.Y., N.L.; Project administration: J. Li, M.-F.L.; Funding acquisition: J. Li, M.-F.L.

Funding

This study was supported by Genome Tagging Project, Fountain-Valley Life Sciences Fund of the University of Chinese Academy of Sciences Education Foundation, and grants from the Ministry of Science and Technology of China, the

Chinese Academy of Sciences, the National Natural Science Foundation of China, and the Shanghai Municipal Commission for Science and Technology (31821004, 2017 YFA0504400, XDB19010204, 17411954900, 31530048, 81672117, 31730062, 16JC1420500, 17JC1400900, 17JC1420100, OYZDJ-SSW-SMC023). Funding was also provided by a Facility-based Open Research Program.

Data availability

ChIP-seq datasets including H3K4me3 ChIP-seq, ub-H2A ChIP-seq and PHF4-FLAG ChIP-seq have been deposited in GEO under accession number GSE112912. RNA-seq data have also been deposited in GEO under accession number GSE119701.

Supplementary information

Supplementary information available online at
http://dev.biologists.org/lookup/doi/10.1242/dev.175547.supplemental

References

Baarends, W. M., Hoogerbrugge, J. W., Roest, H. P., Ooms, M., Vreeburg, J., Hoeijmakers, J. H. J. and Grootegoed, J. A. (1999). Histone ubiquitination and chromatin remodeling in mouse spermatogenesis. *Dev. Biol.* **207**, 322-333. doi:10.1006/dbio.1998.9155

Bao, J. and Bedford, M. T. (2016). Epigenetic regulation of the histone-to-protamine transition during spermiogenesis. *Reproduction* **151**, R55-R70. doi:10.1530/REP-15-0562

Bastos, H., Lassalle, B., Chicheportiche, A., Riou, L., Testart, J., Allemand, I. and Fouchet, P. (2005). Flow cytometric characterization of viable meiotic and postmeiotic cells by Hoechst 33342 in mouse spermatogenesis. *Cytometry A* **65**, 40-49. doi:10.1002/cyto.a.20129

Carrell, D. T. and Aston, K. I. (2013). *Spermatogenesis: Methods and Protocols*. New York: Humana Press.

Casas, E. and Vavouri, T. (2014). Sperm epigenomics: challenges and opportunities. *Front. Genet.* **5**, 330. doi:10.3389/fgene.2014.00330

Chang, Y. F., Lee-Chang, J. S., Panneerdoss, S., MacLean, J. A., II and Rao, M. K. (2011). Isolation of Sertoli, Leydig, and spermatogenic cells from the mouse testis. *BioTechniques* **51**, 341-342, 344. doi:10.2144/000113764

Cho, C., Willis, W. D., Goulding, E. H., Jung-Ha, H., Choi, Y. C., Hecht, N. B. and Eddy, E. M. (2001). Haploinsufficiency of protamine-1 or –2 causes infertility in mice. *Nat. Genet.* **28**, 82-86. doi:10.1038/ng0501-82

Cho, C., Jung-Ha, H., Willis, W. D., Goulding, E. H., Stein, P., Xu, Z., Schultz, R. M., Hecht, N. B. and Eddy, E. M. (2003). Protamine 2 deficiency leads to sperm DNA damage and embryo death in mice. *Biol. Reprod.* **69**, 211-217. doi:10.1095/biolreprod.102.015115

Deshaies, R. J. and Joazeiro, C. A. P. (2009). RING domain E3 ubiquitin ligases. *Annu. Rev. Biochem.* **78**, 399-434. doi:10.1146/annurev.biochem.78.101807.093809

Gou, L. T., Kang, J. Y., Dai, P., Wang, X., Li, F., Zhao, S., Zhang, M., Hua, M. M., Lu, Y., Zhu, Y. et al. (2017). Ubiquitination-deficient mutations in human piwi cause male infertility by impairing histone-to-protamine exchange during spermiogenesis. *Cell* **169**, 1090-1104.e1013. doi:10.1016/j.cell.2017.04.034

Govin, J., Caron, C., Lestrat, C., Rousseaux, S. and Khochbin, S. (2004). The role of histones in chromatin remodelling during mammalian spermiogenesis. *Eur. J. Biochem.* **271**, 3459-3469. doi:10.1111/j.1432-1033.2004.04266.x

Holdcraft, R. W. and Braun, R. E. (2004). Androgen receptor function is required in Sertoli cells for the terminal differentiation of haploid spermatids. *Development* **131**, 459-467. doi:10.1242/dev.00957

Hou, X., Zhang, W., Xiao, Z., Gan, H., Lin, X., Liao, S. and Han, C. (2012). Mining and characterization of ubiquitin E3 ligases expressed in the mouse testis. *BMC Genomics* **13**, 495. doi:10.1186/1471-2164-13-495

Huen, M. S., Grant, R., Manke, I., Minn, K., Yu, X., Yaffe, M. B. and Chen, J. (2007). RNF8 transduces the DNA-damage signal via histone ubiquitylation and checkpoint protein assembly. *Cell* **131**, 901-914. doi:10.1016/j.cell.2007.09.041

Jason, L. J. M., Moore, S. C., Lewis, J. D., Lindsey, G. and Ausio, J. (2002). Histone ubiquitination: a tagging tail unfolds? *BioEssays* **24**, 166-174. doi:10.1002/bies.10038

Kishigami, S., Wakayama, S., Nguyen, V. T. and Wakayama, T. (2004). Similar time restriction for intracytoplasmic sperm injection and round spermatid injection into activated oocytes for efficient offspring production. *Biol. Reprod.* **70**, 1863-1869. doi:10.1095/biolreprod.103.025171

Kouzarides, T. (2007). Chromatin modifications and their function. *Cell* **128**, 693-705. doi:10.1016/j.cell.2007.02.005

Landt, S. G., Marinov, G. K., Kundaje, A., Kheradpour, P., Pauli, F., Batzoglou, S., Bernstein, B. E., Bickel, P., Brown, J. B., Cayting, P. et al. (2012). ChIP-seq guidelines and practices of the ENCODE and modENCODE consortia. *Genome Res.* **22**, 1813-1831. doi:10.1101/gr.136184.111

Leung, J. W., Agarwal, P., Canny, M. D., Gong, F., Robison, A. D., Finkelstein, I. J., Durocher, D. and Miller, K. M. (2014). Nucleosome acidic patch promotes RNF168- and RING1B/BMI1-dependent H2AX and H2A ubiquitination and DNA damage signaling. *PLoS Genet.* **10**, e1004178. doi:10.1371/journal.pgen.1004178

Lu, L.-Y., Wu, J., Ye, L., Gavrilina, G. B., Saunders, T. L. and Yu, X. (2010). RNF8-dependent histone modifications regulate nucleosome removal during spermatogenesis. *Dev. Cell* **18**, 371-384. doi:10.1016/j.devcel.2010.01.010

Meistrich, M. L. and Hess, R. A. (2013). Assessment of spermatogenesis through staging of seminiferous tubules. *Methods Mol. Biol.* **927**, 299-307. doi:10.1007/978-1-62703-038-0_27

Meistrich, M. L., Mohapatra, B., Shirley, C. R. and Zhao, M. (2003). Roles of transition nuclear proteins in spermiogenesis. *Chromosoma* **111**, 483-488. doi:10.1007/s00412-002-0227-z

Oliva, R. (2006). Protamines and male infertility. *Hum. Reprod. Update* **12**, 417-435. doi:10.1093/humupd/dml009

Rathke, C., Baarends, W. M., Awe, S. and Renkawitz-Pohl, R. (2014). Chromatin dynamics during spermiogenesis. *Biochim. Biophys. Acta* **1839**, 155-168. doi:10.1016/j.bbagrm.2013.08.004

Ricke, R. M. and Bielinsky, A.-K. (2005). Easy detection of chromatin binding proteins by the histone association assay. *Biol. Proced. Online* **7**, 60-69. doi:10.1251/bpo106

Rozowsky, J., Euskirchen, G., Auerbach, R. K., Zhang, Z. D., Gibson, T., Bjornson, R., Carriero, N., Snyder, M. and Gerstein, M. B. (2009). PeakSeq enables systematic scoring of ChIP-seq experiments relative to controls. *Nat. Biotechnol.* **27**, 66-75. doi:10.1038/nbt.1518

Sadate-Ngatchou, P. I., Payne, C. J., Dearth, A. T. and Braun, R. E. (2008). Cre recombinase activity specific to postnatal, premeiotic male germ cells in transgenic Mice. *Genesis* **46**, 738-742. doi:10.1002/dvg.20437

Shechter, D., Dormann, H. L., Allis, C. D. and Hake, S. B. (2007). Extraction, purification and analysis of histones. *Nat. Protoc.* **2**, 1445-1457. doi:10.1038/nprot.2007.202

Sheng, K., Liang, X., Huang, S. and Xu, W. (2014). The role of histone ubiquitination during spermatogenesis. *BioMed Res. Int.* **2014**, 870695. doi:10.1155/2014/870695

Shi, X., Hong, T., Walter, K. L., Ewalt, M., Michishita, E., Hung, T., Carney, D., Pena, P., Lan, F., Kaadige, M. R. et al. (2006). ING2 PHD domain links histone H3 lysine 4 methylation to active gene repression. *Nature* **442**, 96-99. doi:10.1038/nature04835

Siklenka, K., Erkek, S., Godmann, M., Lambrot, R., McGraw, S., Lafleur, C., Cohen, T., Xia, J., Suderman, M., Hallett, M. et al. (2015). Disruption of histone methylation in developing sperm impairs offspring health transgenerationally. *Science* **350**, aab2006. doi:10.1126/science.aab2006

Sin, H. S., Barski, A., Zhang, F., Kartashov, A. V., Nussenzweig, A., Chen, J., Andreassen, P. R. and Namekawa, S. H. (2012). RNF8 regulates active epigenetic modifications and escape gene activation from inactive sex chromosomes in post-meiotic spermatids. *Genes Dev.* **26**, 2737-2748. doi:10.1101/gad.202713.112

Wei, L., Wang, X., Yang, S., Yuan, W. and Li, J. (2017). Efficient generation of the mouse model with a defined point mutation through haploid cell-mediated gene editing. *J. Genet. Genomics* **44**, 461-463. doi:10.1016/j.jgg.2017.07.004

Wu, Y., Li, Q. and Chen, X.-Z. (2007). Detecting protein-protein interactions by Far western blotting. *Nat. Protoc.* **2**, 3278-3284. doi:10.1038/nprot.2007.459

Wu, Y., Zhou, H., Fan, X., Zhang, Y., Zhang, M., Wang, Y., Xie, Z., Bai, M., Yin, Q., Liang, D. et al. (2015). Correction of a genetic disease by CRISPR-Cas9-mediated gene editing in mouse spermatogonial stem cells. *Cell Res.* **25**, 67-79. doi:10.1038/cr.2014.160

Xiao, J., Xu, M., Li, J., Chang Chan, H., Lin, M., Zhu, H., Zhang, W., Zhou, Z., Zhao, B. and Sha, J. (2002). NYD-SP6, a novel gene potentially involved in regulating testicular development/spermatogenesis. *Biochem. Biophys. Res. Commun.* **291**, 101-110. doi:10.1006/bbrc.2002.6396

Yang, H., Shi, L., Chen, C. D. and Li, J. (2011). Mice generated after round spermatid injection into haploid two-cell blastomeres. *Cell Res.* **21**, 854-858. doi:10.1038/cr.2011.45

Yang, H., Shi, L., Wang, B.-A., Liang, D., Zhong, C., Liu, W., Nie, Y., Liu, J., Zhao, J., Gao, X. et al. (2012a). Generation of genetically modified mice by oocyte injection of androgenetic haploid embryonic stem cells. *Cell* **149**, 605-617. doi:10.1016/j.cell.2012.04.002

Yang, S. Y., Baxter, E. M. and Van Doren, M. (2012b). Phf7 controls male sex determination in the Drosophila germline. *Dev. Cell* **22**, 1041-1051. doi:10.1016/j.devcel.2012.04.013

Zhang, M., Zhou, H., Zheng, C., Xiao, J., Zuo, E., Liu, W., Xie, D., Shi, Y., Wu, C., Wang, H. et al. (2014). The roles of testicular c-kit positive cells in de novo morphogenesis of testis. *Sci. Rep.* **4**, 5936. doi:10.1038/srep05936

Zhong, C., Yin, Q., Xie, Z., Bai, M., Dong, R., Tang, W., Xing, Y.-H., Zhang, H., Yang, S., Chen, L.-L. et al. (2015). CRISPR-Cas9-mediated genetic screening in mice with haploid embryonic stem cells carrying a guide RNA library. *Cell Stem Cell* **17**, 221-232. doi:10.1016/j.stem.2015.06.005

Supplementary Figures

Figure S1.

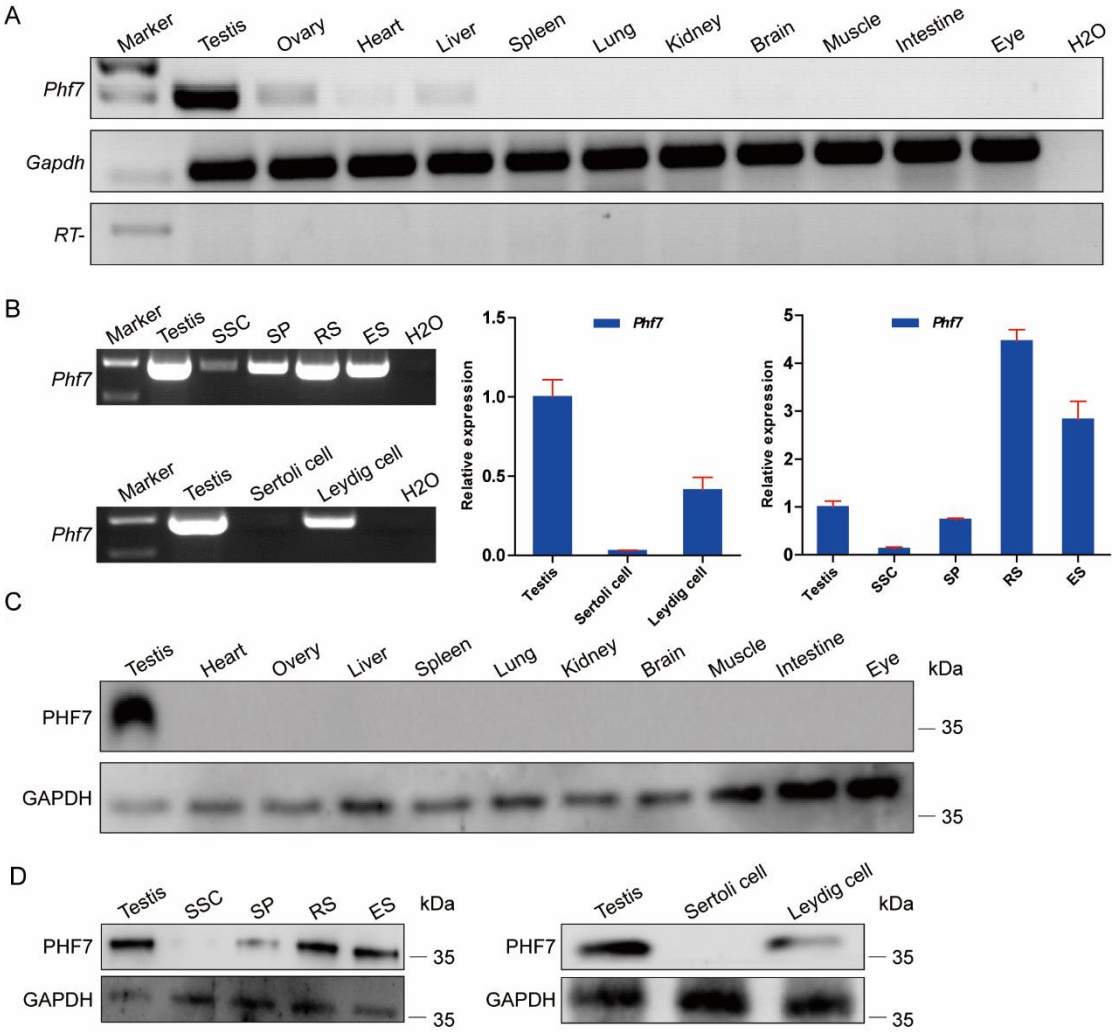

Figure S1. PHF7 is Specifically Expressed in Spermatids.

(A) Determination of *Phf7* transcript levels in different tissues by qPCR. *RT-* represents RNA used as the template in PCR reactions.

(B) Determination of *Phf7* transcript levels in different testicular cells by real-time quantitative PCR (RT-qPCR). The left panels show the representative electrophoresis images of RT-qPCR results, and the last lane (H2O) is the blank control. The right two panels are the quantitative results from the left panels,

normalized to the average transcript level of *Phf7* in testis. SSC, spermatogonial stem cells; SP, spermatocytes; RS, round spermatids; ES, elongating spermatids.

(C) Western blot of PHF7 in different tissues. The tissues were dissociated from WT mice and treated in lysis buffer for SDS-PAGE gels, with GAPDH as a loading control.

(D) Western blot of PHF7 in different testicular cells with GAPDH as a loading control.

Figure S2.

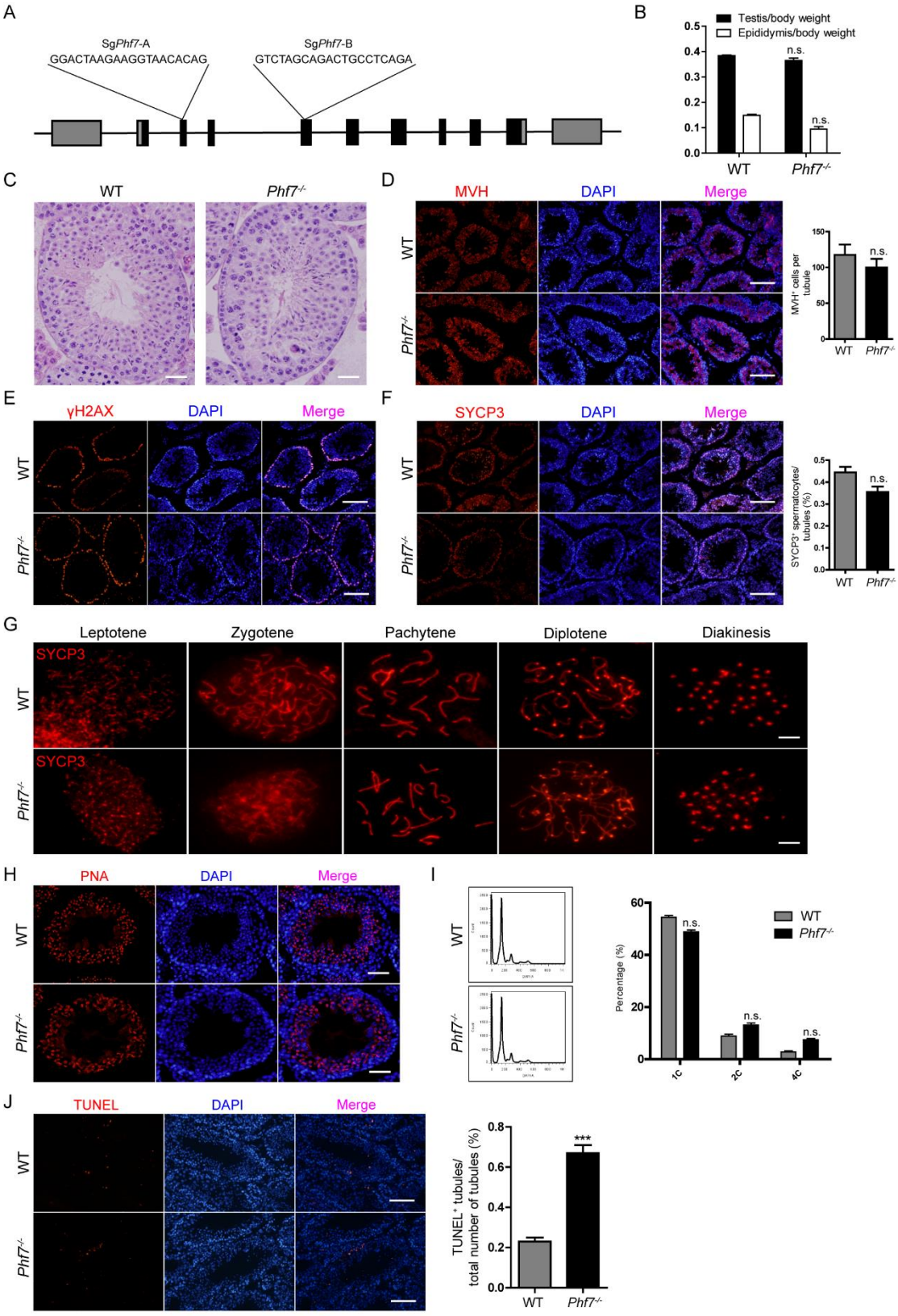

Figure S2. Generation and Characterization of *Phf7* Mutant Mice.

(A) Schematic for CRISPR-Cas9-mediated *Phf7* knockout in mice. SgRNA-A and sgRNA-B were designed to target exon 2 and 4 of *Phf7*, respectively.

(B) Comparison of testis/body and epididymis/body weight between WT and *Phf7*$^{-/-}$ mice. The average values ± SD of three separate experiments are plotted. n.s., not significant.

(C) Representative H&E staining images of WT and *Phf7*$^{-/-}$ testis. Scale bar, 50 μm.

(D) Immunostaining of MVH (red) in testis sections from 8-week-old WT and *Phf7*$^{-/-}$ mice with nuclei counterstained with DAPI (blue). The number of MVH^{+} cells *per* tubule are shown in the right panel. n.s., not significant. Scale bar, 100 μm.

(E) Immunostaining of γH2A (red) in testis sections from WT and *Phf7*$^{-/-}$ 8-week-old mice. Scale bar, 100 μm.

(F) Immunostaining of SYCP3 (red) in testis sections from WT and *Phf7*$^{-/-}$ 8-week-old mice. The ratios of SYCP3^{+} spermatocytes *per* tubule are shown in the right panel. n.s., not significant. Scale bar, 100 μm.

(G) SYCP3 antibody (red) immunostaining of meiotic chromosome spreads of spermatocytes at different stages. Scale bar, 100 μm.

(H) Immunostaining of PNA in WT and *Phf7*$^{-/-}$ testes from 8-week-old mice. Testis sections were stained with PNA (red) to indicate acrosome formation. Nuclei were stained with DAPI (blue). Scale bar, 50 μm.

(I) FACS analysis of the ratio of haploid cells in testes from WT and *Phf7*$^{-/-}$ 8-week-old mice. The percentage of 1C, 2C, and 4C cells in the testes are shown in the right panel. n.s., not significant.

(J) TUNEL assay of testis sections from 8-week-old *Phf7*$^{-/-}$ and WT mice. Testis sections were stained with TUNEL (red) to indicate apoptosis. Nuclei were stained with DAPI (blue). The number of TUNEL^{+} tubules and the total number of tubules are shown in the right panel. ***, $P < 0.001$. Scale bar, 50 μm.

Figure S3.

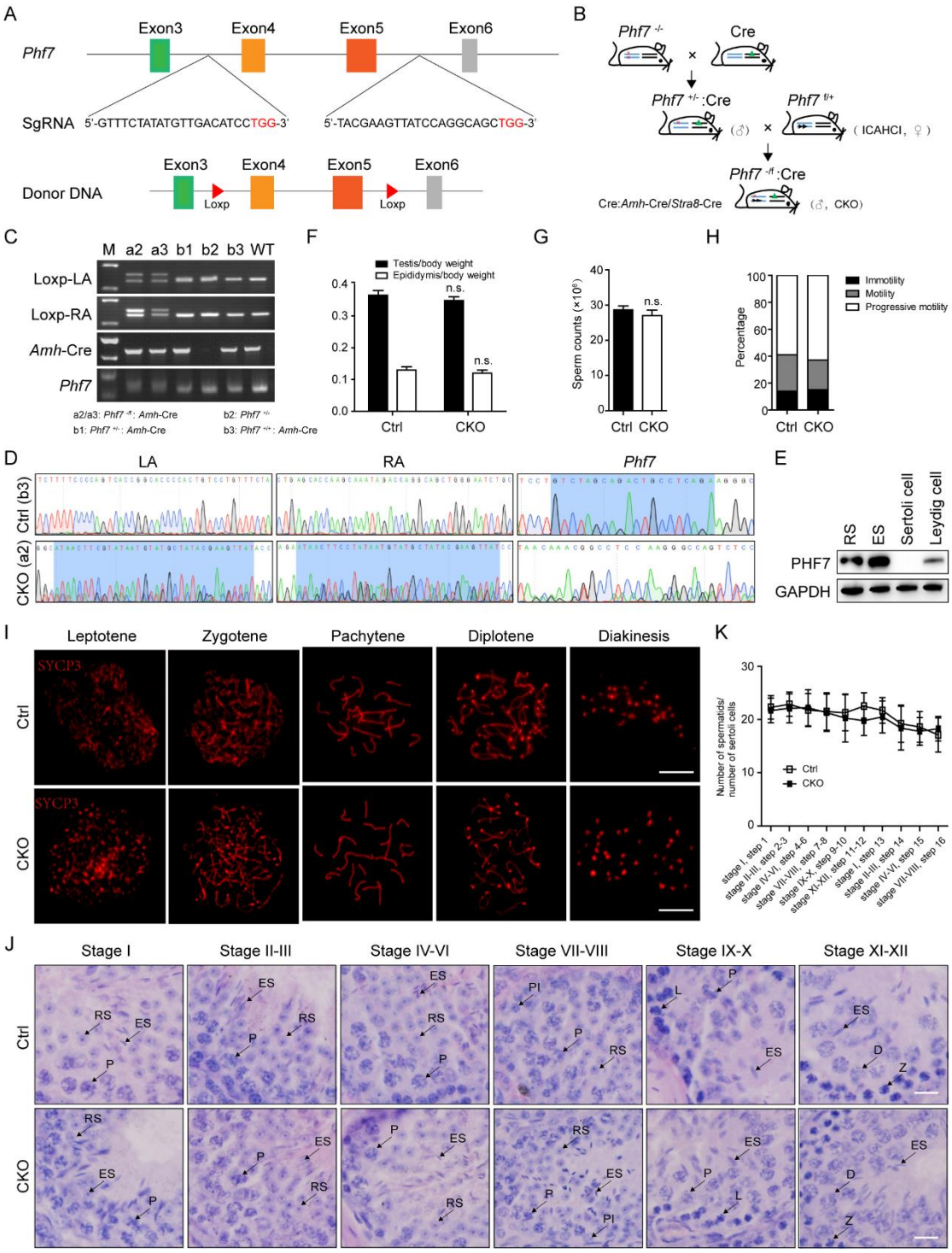

Figure S3. Generation and Characterization of Mice Carrying Mutant *Phf7* in Sertoli Cells.

(A) A schematic illustrating the construction of *Phf7*-loxp mice. The donor DNA with Loxp sequences was knocked into targeted loci to abolish exon 4 and 5 of *Phf7*. The sequences of two sgRNAs are shown and the PAM is marked in red.

(B) A schematic illustrating the generation of conditional knockout mice by crossing *Phf7*-Loxp mice with mice carrying a *Cre* transgene .

(C) PCR analysis of tail DNA from mice obtained by crossing *Phf7*-Loxp mice with *Amh*-Cre mice. LA and RA represent the left and right arm of Loxp, respectively. a2, a3, b1, b2, and b3 represent the different pups.

(D) DNA sequences of PCR products (C) amplified from the LA, RA, and *Phf7* locus in two mice (a2 and b3), respectively. Two peaks can be observed in the LA, RA and *Phf7* locus of mouse a2 (CKO), while only one peak can be observed in mouse b3 (control).

(E) Western blot of PHF7 in different testicular cells from mouse a2 (CKO). GAPDH is a loading control.

(F) Comparison of the ratios of testis/body and epididymis/body weight between 10-week-old CKO and control littermates. The average values ± SD of three separate experiments are plotted. n.s., not significant.

(G) Sperm counts in cauda epididymes from 10-week-old CKO and control mice. n.s., not significant.

(H) CASA analysis of immotility, motility, and progressive motility of sperm from 10-week-old CKO mice generated by *Amh*-Cre.

(I) SYCP3 antibody (red) immunostaining of meiotic chromosome spreads of spermatocytes from 10-week-old CKO mice at different stages. Scale bar, 10 μm.

(J) H&E staining of testis sections from 8-week-old mice carrying mutant *Phf7* in Sertoli cells. Stages of seminiferous epithelium cycles were determined by

morphology of spermatocytes and round spermatids. PI, preleptotene; L, leptotene; Z, zygotene; P, pachytene; D, diplotene; RS, round spermatids; ES, elongating spermatids. Scale bar, 20 μm.

(K) The number of spermatids at different stages are comparable between CKO and control littermate mice during spermiogenesis. Ratios are of spermatids and Sertoli cells in tubule cross sections from specific stages of the seminiferous epithelial cycles and corresponding spermatid development steps are shown.

Figure S4.

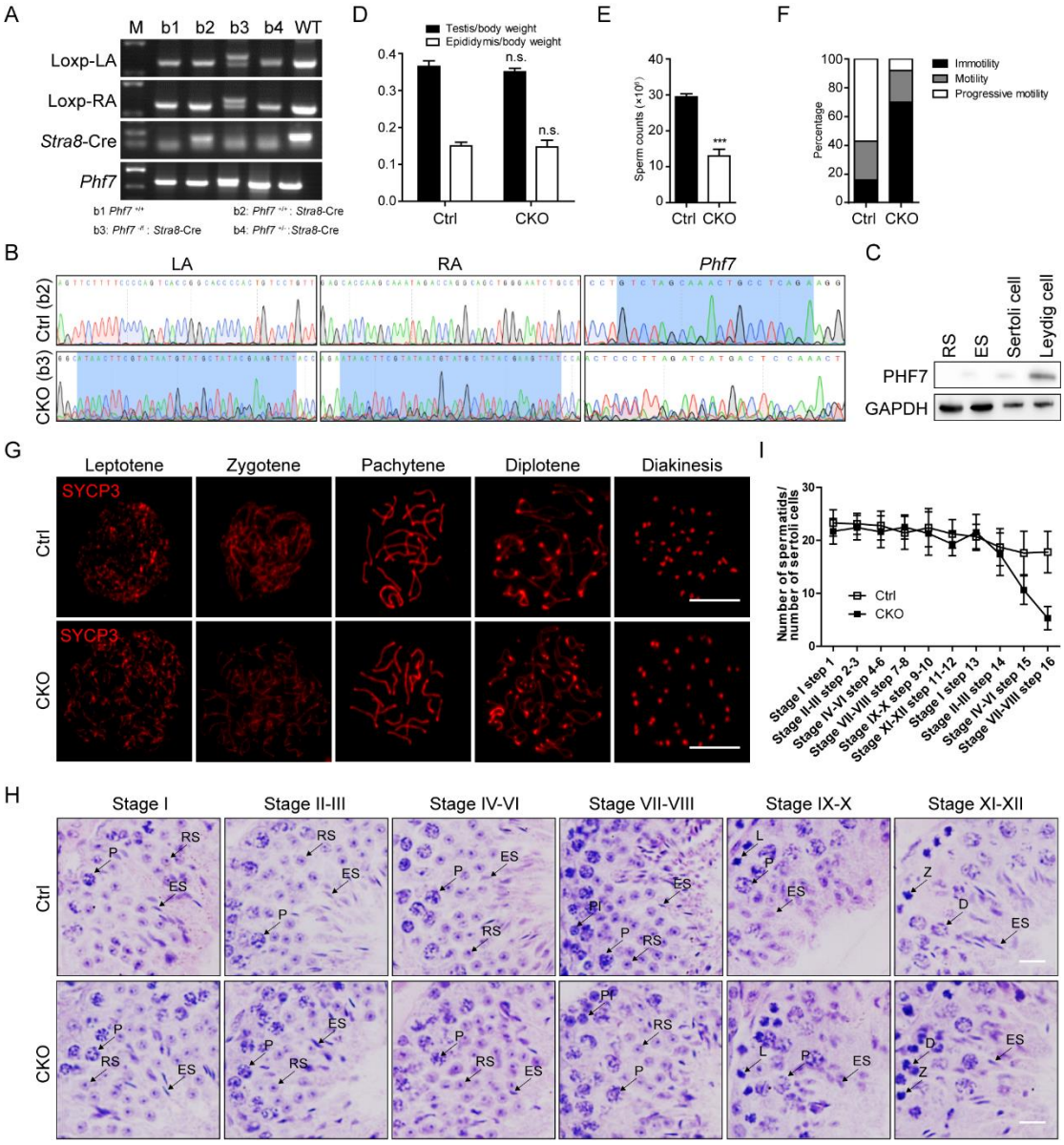

Figure S4. Generation and Characterization of Mice Carrying Mutant *Phf7* in Germ Cells.

(A) PCR analysis of tail DNA from mice obtained by crossing *Phf7*-Loxp mice with *Stra8*-Cre mice. LA and RA represent the left and right arm of Loxp, respectively. b1, b2, b3, and b4 represent the different pups.

(B) DNA sequences of PCR products (A) amplified from the LA, RA and *Phf7* locus in two mice (b2 and b3), respectively. Two peaks can be observed in the LA, RA and *Phf7* locus of mouse b3 (CKO), while only one peak is observed in mouse b2 (control).

(C) Western blot of PHF7 in different testicular cells from mouse b3 (CKO). GAPDH is a loading control.

(D) Comparison of the ratios of testis/body or epididymis/body weight between a 10-week-old CKO mouse (b3) and control littermate (b2). The average values ± SD of three separate experiments are plotted. n.s., not significant.

(E) Sperm counts in the cauda epididymis from 10-week-old CKO (b3) and control (b2) mice. ***, $P < 0.001$.

(F) CASA analysis of immotility, motility, and progressive motility of sperm from 10-week-old CKO mice generated by *Stra8*-Cre.

(G) SYCP3 antibody immunostaining (red) of meiotic chromosome spreads of spermatocytes from 10-week-old CKO mice carrying mutant *Phf7* in germ cells at different stages. Scale bar, 10 μm.

(H) H&E staining of testis sections from 8-week-old mice carrying mutant *Phf7* in germ cells. Stages of seminiferous epithelium cycles were determined by morphology of spermatocytes and round spermatids. PI, preleptotene; L, leptotene; Z, zygotene; P, pachytene; D, diplotene; RS, round spermatids; ES, elongating spermatids. Scale bar, 20 μm.

(I) A reduced number of spermatids was observed in mice carrying mutant *Phf7* in germ cells. Ratios between spermatids and Sertoli cells in tubule cross sections of specific stages of seminiferous epithelial cycles and corresponding spermatid development steps are shown.

Figure S5.

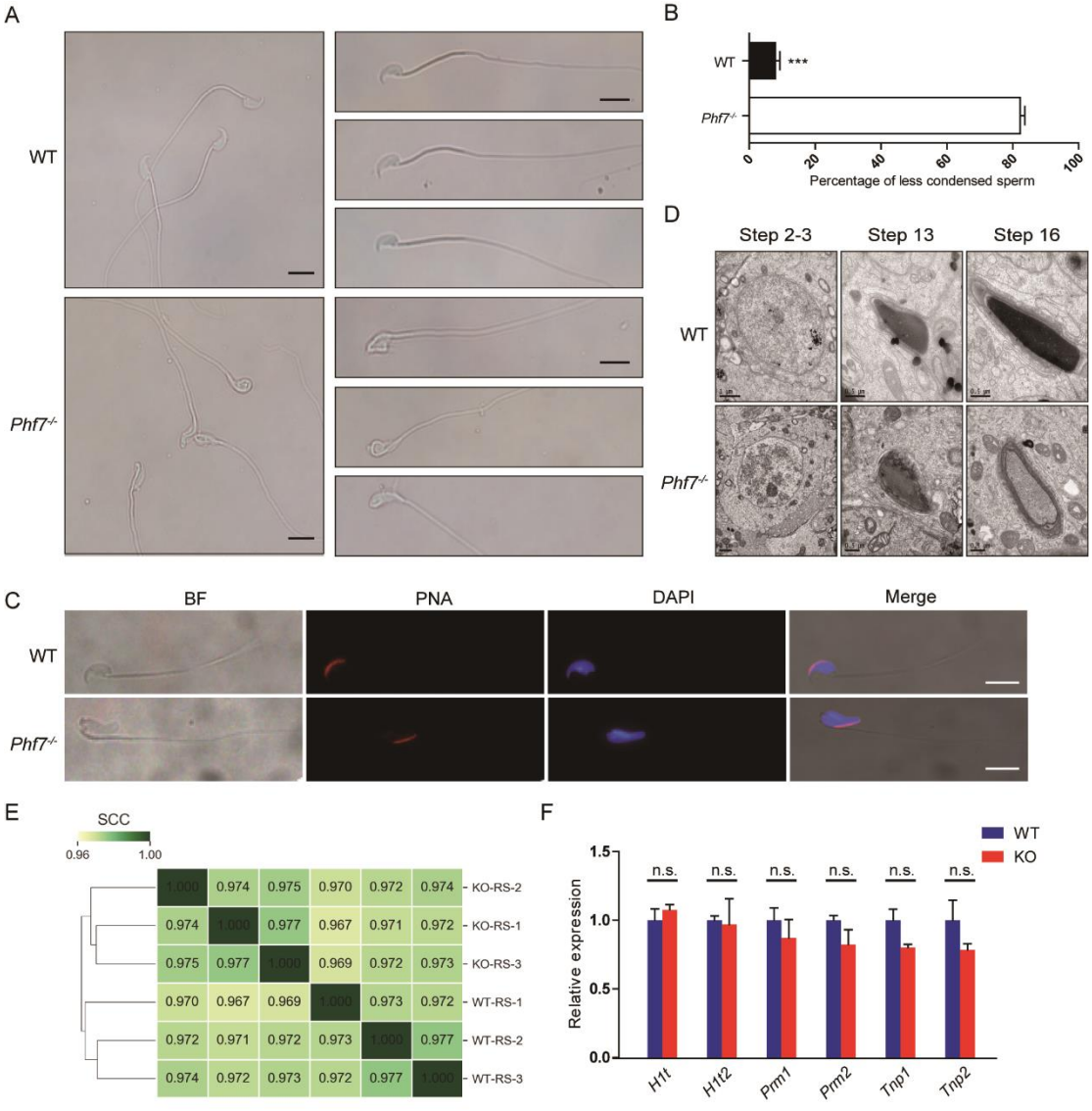

Figure S5. Abnormal Chromatin Compaction in *Phf7* Mutant Sperm and The Transcriptional Profile of WT and *Phf7* Knockout Round Spermatids.

(A) Sperms from *Phf7*$^{-/-}$ mice showed abnormal morphology in head. Representative differential interference contrast (DIC) images of sperm from 8-week-old mutant (bottom) and WT (upper) mice. Scale bar, 10 μm.

(B) Quantification of sperm with less condensed nuclei in *Phf7*$^{-/-}$ and WT males.

n=100 per group; the average values ± SD of three separate experiments are plotted. ***, $P < 0.001$.

(C) Immunostaining of PNA in sperm isolated from WT and *Phf7* knockout epididymes. Sperm were stained with PNA (red) to indicate acrosome formation. Nuclei were stained with DAPI (blue). Scale bar, 10 μm.

(D) Representative transmission electron micrograph images of mutant and WT spermatids at different stages from 10-week-old mice. Chromatin condensation in *Phf7*$^{-/-}$ spermatids gradually becomes defective from step 13 to 16.

(E) Clustered correlation heatmap of *Phf7* knockout and WT RNA-seq samples (three replicates per condition). Spearman correlation coefficients were calculated based on the expression values (FPKM) of all RefSeq annotated genes.

(F) Quantitative PCR analysis of histone-to-protamine exchange related genes from WT and *Phf7* knockout round spermatids. ***, $P < 0.001$. n.s., not significant.

Figure S6.

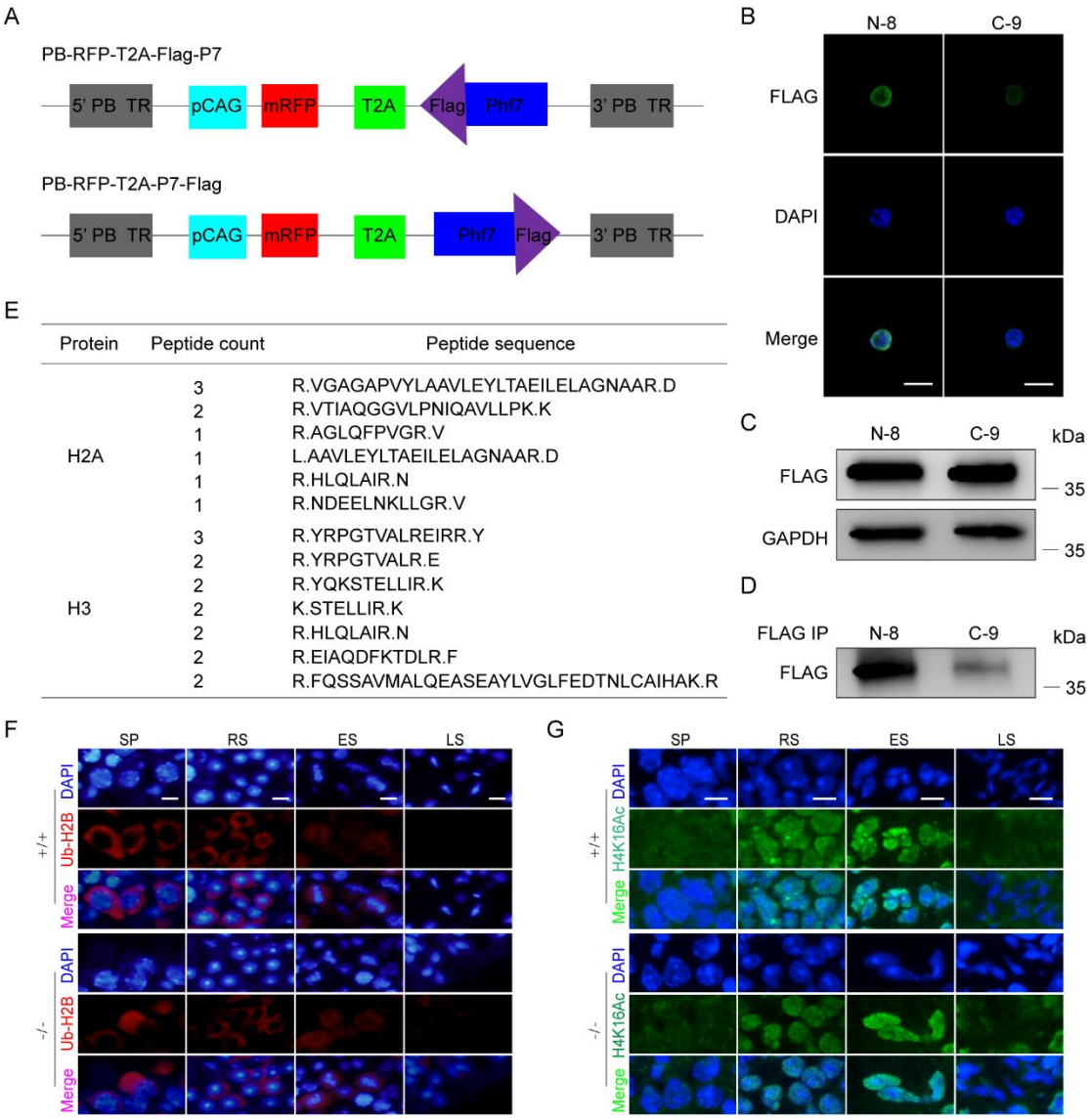

Figure S6. Generation of PHF7 Transgenic Cell Lines and Functional Analysis of *Phf7* Knockout Spermatids.

(A) The schematic of the plasmids constructed for the generation of transgenic haESC lines stably expressing N- or C- terminal Flag-tagged PHF7. Top, PB-RFP-T2A-Flag-Phf7 vector for expressing N-terminal Flag-tagged PHF7. Bottom, PB-RFP-T2A-Phf7-Flag vector for expressing C-terminal Flag-tagged PHF7.

(B) Immunofluorescent analysis of expressed PHF7 using Flag antibody (green), showing nuclear localization of PHF7 in transgenic cells. Nuclei were stained with DAPI (blue). N-8 or C-9 represents cells carrying PB-RFP-T2A-Flag-Phf7 or PB-RFP-T2A-Phf7-Flag transgenes, respectively. Scale bar, 10 μm.

(C) Western blot analysis of PHF7 expression in two transgenic cell lines (N-8 and C-9) using Flag antibody, with GAPDH as a loading control.

(D) Immunoprecipitation (IP) analysis in two transgenic cell lines using anti-Flag beads. Anti-Flag IP pellets were immunoblotted by anti-Flag antibody.

(E) Mass spectrum (MS) analysis of IP pellets in (D). The table shows the detected peptides sequences from proteomic analysis of the IP pellet from N-8.

(F) Immunostaining of ub-H2B (red) in testis sections from 8-week-old *Phf7* knockout and WT males. Nuclei were stained with DAPI (blue). Scale bar, 10 μm.

(G) Immunostaining of H4K16Ac (green) in testis sections from 8-week-old *Phf7* knockout and WT males. Nuclei were stained with DAPI (blue). Scale bar, 10 μm.

Figure S7.

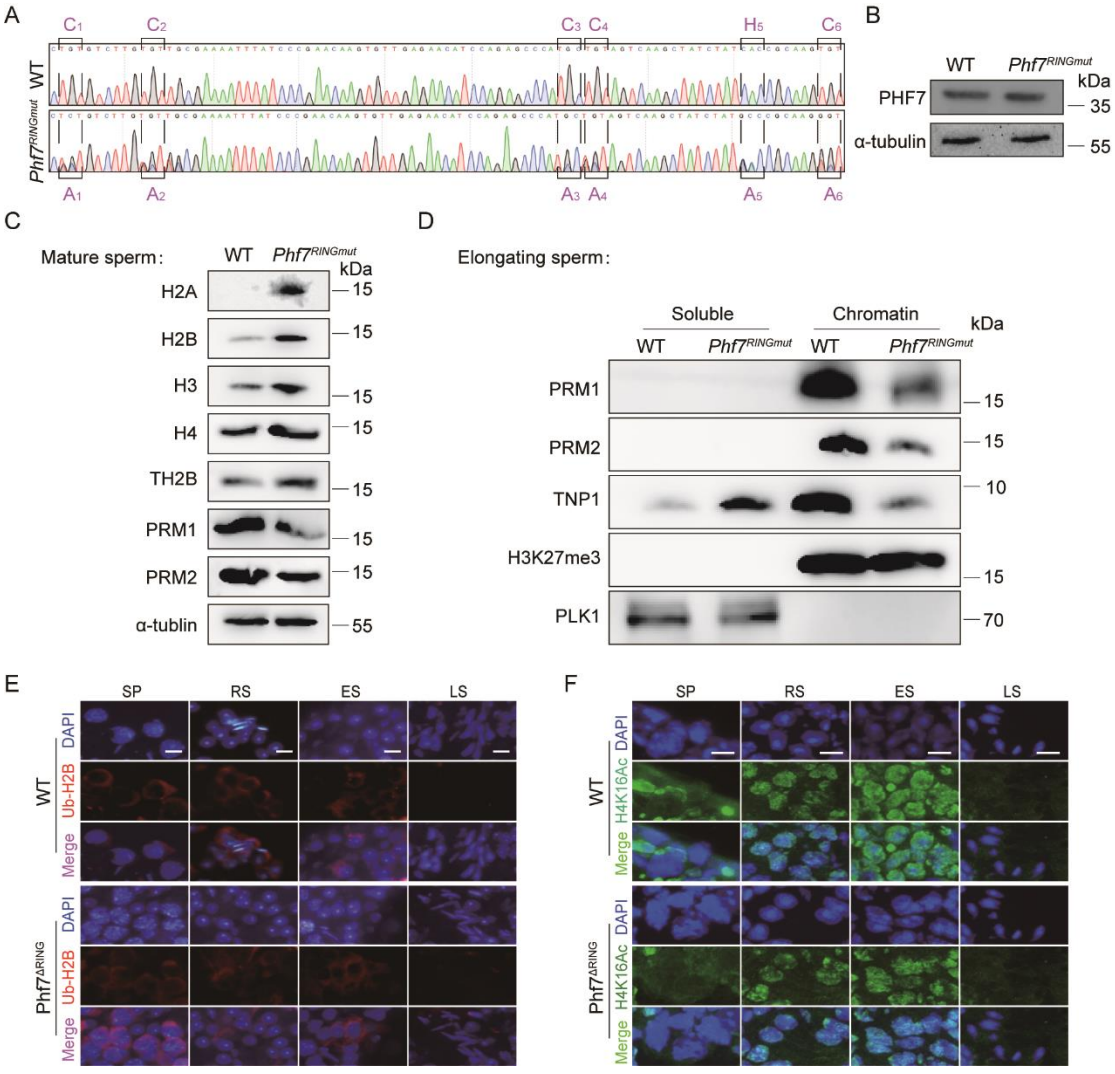

Figure S7. Function Analysis of PHF7 with a Mutant RING Domain *in vitro* and *in vivo*.

(A) DNA sequence of PCR products amplified from the *Phf7* RING domain.

(B) Western blot analysis of PHF7 expression in haploid spermatids from 8-week-old *Phf7*^{RINGmut} and WT mice, with α-tubulin as a loading control.

(C) Western blot analysis of histones and protamines in mature sperm from the

epididymes of 12-week-old *Phf7*^{RINGmut} and WT mice, with α-tubulin as a loading control.

(D) Western blot analysis of protamines and transition protein (TNP1) in soluble or chromatin-bound in elongating spermatids from 8-week-old *Phf7*^{RINGmut} and WT mice. PLK1 and H3K27me3 served as controls for soluble and chromatin fractions, respectively.

(E) Immunostaining of ub-H2B (red) in testis sections from an 8-week-old *Phf7* mouse carrying mutant RING domain (*Phf7*^{RINGmut}). Nuclei were stained with DAPI (blue). Scale bar, 10 µm.

(F) Immunostaining of H4K16Ac (red) in testis sections from an 8-week-old *Phf7* mouse carrying mutant RING domain (*Phf7*^{RINGmut}). Nuclei were stained with DAPI (blue). Scale bar, 10 µm.

Figure S8.

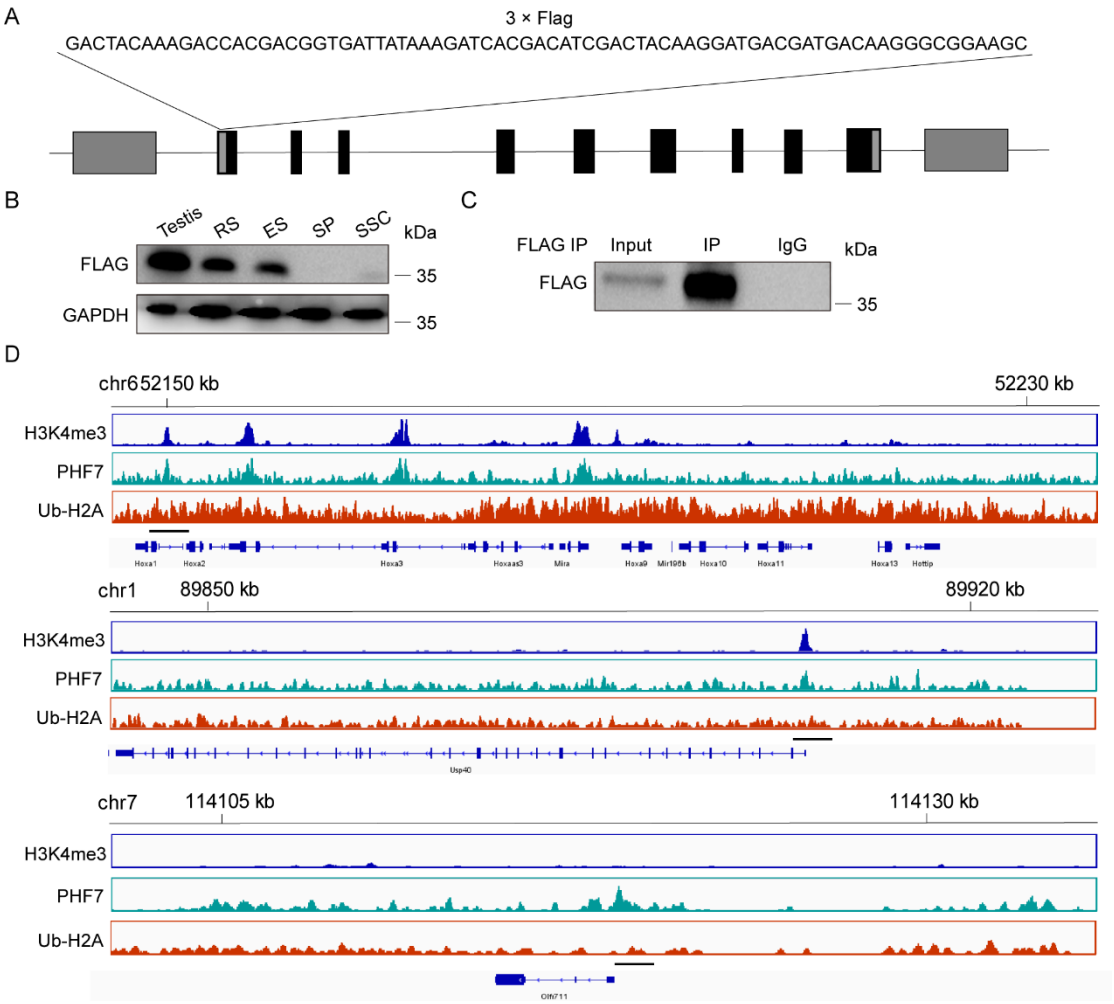

Figure S8. Generation and Characterization of *Phf7*-flag Knockin Mice.

(A) A schematic diagram illustrating the knockin position of the *Flag* sequence. The 3 × *Flag* was knocked into the N-terminus of *Phf7*.

(B) Western blot analysis of PHF7 in different testicular cells of knockin mice, showing specific expression of PHF7 in round spermatids (RS) and elongating sperm (ES). GAPDH served as a loading control.

(C) Immunoprecipitation (IP) analysis in Flag-knockin spermatids using anti-Flag beads. Flag-IP pellets were immunoblotted by anti-Flag antibody. Left lane, input load represents 10% of total. Middle lane, Flag IP pellets. Right lane, IgG IP as a negative control.

(D) Representative peaks overlapping with H3K4me3 and PHF7 in three gene loci from ChIP-seq. Top, *Hoxa* cluster; an example of peaks overlapping with H3K4me3 and PHF7. The region enriched with ub-H2A around the TSS is underlined. Middle, *Usp40* locus; an example of a peak unique to H3K4me3. Ub-H2A is less enriched in the underlined region. Bottom, *Olfr711* locus; an example of a peak unique to PHF7. Ub-H2A is less enriched in the underlined region..

Figure S9.

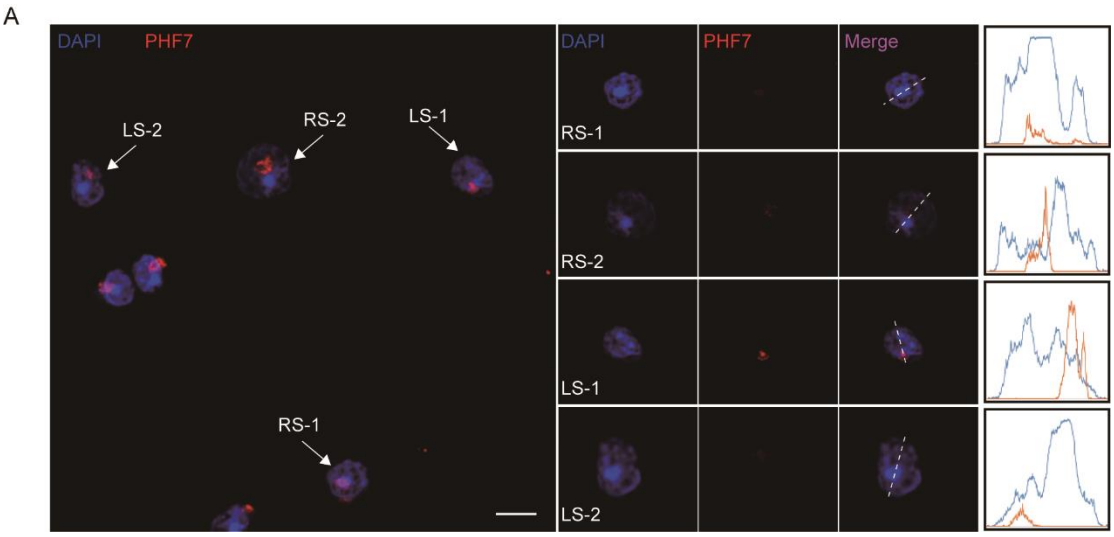

Figure S9. The nuclear localization of PHF7 in spermatids.

(A) Immunofluorescent images of spermatids stained for PHF7 (red) isolated from 8-week-old WT mice. Nuclei are counterstained by DAPI (blue). Arrows in the left image indicate round spermatids (RS) and late spermatids (LS) that are magnified in right lanes. Right lanes, areas of co-localization of red and blue signals are shown by line intensity. Scale bar, 10 μm.

Table S1. Summary of ROSI experiments

Round spermatids	No. of 2-cell Embryo Transfer	No. of Pups	Birth Rate (%)
WT	146	45	30.28
Phf7$^{-/-}$	86	28	32.56

Table S2. *In vitro* Development of Embryos by ICSI

Sperm	No. of oocytes	No. of 2-cell embryos	No. of blastocysts	Rate of 2-cell (%)	Rate of blastocyst (%)
WT	83	78	40	93.98	51.28
Phf7$^{-/-}$	93	61	2	65.59	3.28

Table S3. Key resource table

REAGENT or RESOURCE	SOURCE	IDENTIFIER
Antibodies		
Rabbit polyclonal anti-PHF7	Abcam	ab179660
Rabbit polyclonal anti-RNF8	Proteintech	Cat#14112-1-AP
Rabbit polyclonal anti-TNP1	Proteintech	Cat#17178-1-AP;RRID:AB_2206757
Goat polyclonal anti-PRM1	Santa Cruz	sc-23107; RRID:AB_2171310
Goat polyclonal anti-PRM2	Santa Cruz	sc-23104; RRID:AB_2284440
Mouse monoclonal anti-a-gapdh	Cell Signaling Technology	#2118
Mouse monoclonal anti-a-tubulin	Sigma	T6199
Mouse monoclonal anti-H3K4me1	Active motif	39635
Mouse monoclonal anti-H3K4me2	Active motif	39679
Mouse polyclonal anti-H3K4me3	Active motif	39916
Mouse polyclonal anti-H3K27me3	Millipore	07-449
Rabbit polyclonal anti-Plk1	Proteintech	10305-1-AP
Rabbit polyclonal anti-H4K16Ac	Abcam	Ab109463
Mouse monoclonal anti-Ub	Santa Cruz	sc-8017; RRID: AB_628423
Rabbit polyclonal anti-H2A	Cell Signaling Technology	Cat#12349
Rabbit polyclonal anti-H2B	Cell Signaling Technology	Cat#12364
Rabbit polyclonal anti-H3	Cell Signaling Technology	Cat#9715; RRID:AB_331563
Rabbit polyclonal anti-H4	Cell Signaling Technology	Cat#13919
Rabbit polyclonal anti-ub-H2A	Millipore	Cat#ABE569
Rabbit polyclonal anti-ub-H2B	Cell Signaling Technology	Cat#5546;RRID:AB_10693452
Goat anti-rabbit poly-HRP	Thermo scientific	32260
Goat anti-mouse poly-HRP	Thermo scientific	32230
Mouse monoclonal anti-Mvh	Abcam	ab27591
Rabbit polyclonal anti-Sycp3	Abcam	ab15093
Rabbit polyclonal anti-γH2A.X	Abcam	ab11174
Mouse monoclonal anti-Flag	Sigma	Cat#F3165; RRID: AB_259529
Rabbit polyclonal anti-GST	ABclonal Technology	Cat#AE006
Mouse monoclonal anti-Streptavidin	Thermo scientific	MA5-17282
Chemicals, Peptides, and Recombinant Proteins		
Hematoxylin and Eosin	Shanghai hongqiao lexiang medical reagent technology co., LT	N/A
Dynabeads™ Protein G	Thermo Fisher	REF10004D
ANTI-FLAG M2 affinity gel	sigma	A2220
GST•Bind™ Resin	millipore	70541-5

Strep-Tactin® Sepharose® 50% suspension	IBA	2-1201-025
d-Desthiobiotin	sigma	D1411-500MG
L-Glutathione reduced	sigma	G4251-1G
BugBuster® Master Mix	millipore	71456-3
Histone H3 (1-21)	ANAspec	AS-61702
H3K4me1 (1-21)	ANAspec	64355-025
H3K4me2 (1-21)	ANAspec	AS-64356-025
H3K4me3 (1-21)	ANAspec	AS-64357-025
Human, Recombinant Histone H2A	New England BioLabs	Cat#M2502S
Human, Recombinant Histone H2B	New England BioLabs	Cat#M2505S
UbcH5a	Boston Biochem	Cat#E2-616
UbcH5c	Boston Biochem	Cat#E2-802
GST	Purification	N/A
GST-PHF7	Purification	N/A
GST-PHF7$^{\Delta RING}$	Purification	N/A
His-RNF8	Purification	N/A
Strep-PHF7	Purification	N/A
Strep-PHF7$^{\Delta RING}$	Purification	N/A
Strep-PHF7$^{\Delta PHD}$	Purification	N/A
Strep-PHF7$^{\Delta RING\Delta PHD}$	Purification	N/A
Critical Commercial Assays		
QIAquick PCR purification Kit	Qiagen	Cat#28104
MEGAclear™ Kit Purification for Large Scale Transcription Reactions	Life Technologies	AM1908
MEGAshortscript™ Kit	Life Technologies	AM1354
mMESSAGE mMACHINE® T7 Ultra Kit	Life Technologies	AM1345
NEBNext Ultra DNA Library Prep Kit for Illumina	NEB	E7370
MEGAclear™ Kit Purification for Large Scale Transcription Reactions	Life Technologies	AM1908
Deposited Data		
H3K4me3 ChIP-seq	This paper	GSE112912
Ub-H2A ChIP-seq	This paper	GSE112912
Phf7-flag ChIP-seq	This paper	GSE112912
RNA-seq	This paper	GSE119701
Experimental Models: Cell Lines		
HEK293T	American Type Culture Collection	N/A
AG-haESCS	Zhong et al.,2016	N/A
Experimental Models: Organisms/Strains		
Phf7 KO	This paper	

Stra8-Cre	Robert et al.,2003	
Amh-Cre	Patricia et al.,2008	
Phf7-loxp: *Stra8*-Cre	This paper	
Phf7-loxp: *Amh*-Cre	This paper	
Phf7-KI-flag	This paper	
Phf7 ^{RINGmut}	This paper	
Oligonucleotides		
Test-PHF7-AF: GATAGTTGCCAACAGTAGTG	This paper	N/A
Test-PHF7-AR: CTGTAGTCAGGAAGCATCTT	This paper	N/A
Test-PHF7-BF: ATACACAGATGAGTTCCACCAAG	This paper	N/A
Test-PHF7-BR: TCAAGGACACAAGCACATAGG	This paper	N/A
Phf7-flag-check-F: TCTCTAACTCAGTCTCCTCAA	This paper	N/A
Phf7-flag-check-R: TCACCTACTCTACCTCAATCT	This paper	N/A
Phf7-CDS-F: AAGACTTTAAAAGAAAAAAACAAA CATCCAAG	This paper	N/A
Phf7-CDS-R: TTAACTCGTGGTTGAAGCAGGC	This paper	N/A
Phf7-LOXP-Genotyping-AF: AGTGCTGGTGTATCCAATT	This paper	N/A
Phf7-LOXP-Genotyping-AR: CACACGGATTCTGAACATG	This paper	N/A
Phf7-LOXP-Genotyping-BF: GCTGCTCATAACTGAATAGG	This paper	N/A
Phf7-LOXP-Genotyping-BR: GGCTCTGGATGTTCTCAA	This paper	N/A
Recombinant DNA		
pMD19T-PHF7-CDS	This paper	N/A
PB-RFP-T2A-flag-PHF7	This paper	N/A
PB-RFP-T2A -PHF7-flag	This paper	N/A
pGEX6P-1-PHF7	This paper	N/A
pET-51b-PHF7	This paper	N/A
pET-51b-RNF8	This paper	N/A
pGEX6P-1-PHF7$^{\triangle RING}$	This paper	N/A
pET-51b-PHF7$^{\triangle RING}$	This paper	N/A
pET-51b-PHF7$^{\triangle PHD}$	This paper	N/A
pET-51b-PHF7$^{\triangle RING\triangle PHD}$	This paper	N/A

Software and Algorithms		
ImageJ	N/A	https://imagej.nih.gov/ij/download.html
FlowJo V10.2	N/A	https://www.flowjo.com/
GraphPad Prism	N/A	https://www.graphpad.com/
Python 2.7	N/A	https://www.python.org/download/releases/2.7/
macs2 version 1.3.7.1	Zhang et al., 2008	https://github.com/taoliu/MACS
Bowtie version 1.2.1.1	Langmead et al., 2009	http://bowtie-bio.sourceforge.net/index.shtml